Survey of top quark polarization at a polarized linear e^+e^- collider

S. Groote

Loodus- ja Tehnoloogiateaduskond, Füüsika Instituut, Tartu Ülikool, Riia 142, EE51014 Tartu, Estonia

J. G. Körner

Institut für Physik der Johannes-Gutenberg-Universität, Staudinger Weg 7, D-55099 Mainz, Germany

B. Melić

Rudjer Bošković Institute, Theoretical Physics Division, Bijenička c. 54, HR-10000 Zagreb, Croatia

S. Prelovsek

Physics Department at University of Ljubljana and Jozef Stefan Institute, SI-1000 Ljubljana, Slovenia

We discuss in detail top quark polarization in above-threshold ($t\bar{t}$) production at a polarized linear e^+e^- collider. We pay particular attention to the minimization and maximization of the polarization of the top quark by tuning the longitudinal polarization of the e^+ and e^- beams. The polarization of the top quark is calculated in full next-to-leading order QCD. We also discuss the beam polarization dependence of the longitudinal spin-spin correlations of the top and antitop quark spins.

PACS numbers: 13.88.+e, 12.38.Bx, 14.65.Ha

I. INTRODUCTION

A future linear e^+e^- collider offers the cleanest conditions for studying top quark properties, such as the top quark mass, its vector and axial couplings, and possible magnetic and electric dipole moments. Apart from these static properties, also the polarization of the top quark can be studied with great precision. The top decays sufficiently fast so that hadronization effects do not spoil the polarization which it has at its birth. The large number of top quark pairs expected to be produced at the ILC, e.g., 50 ($t\bar{t}$)/hour at 500 GeV (based on a luminosity of $L = 2 \times 10^{34}$ cm^{-2} s^{-1} [1,2]), will enable one to precisely determine the top quark polarization from an angular analysis of its decay products in the dominant decay $t \rightarrow X_b + W^+$. The expected statistical errors in the angular analysis are below the 1% level. Therefore very precise measurements of the angular distributions and correlations of the decay products of t and $\bar{t}$ will shed light on the polarization of the top quarks and on the spin-spin correlations of the top and antitop quark pairs which are imprinted on the top and antitop quarks by the ($t\bar{t}$)-production mechanism. In addition, the measurement of the top polarization will make it possible to precisely determine the electroweak standard model (SM) parameters or to study a variety of new phenomena beyond the SM.

It is well known that the top quarks from e^+e^- annihilations are polarized even for unpolarized e^+e^- beams due to the presence of parity-violating interactions in the standard model (SM). One also knows from the work of Refs. [3,4] that the polarization of the top quark in polarized e^+e^- annihilations can become quite large when the beam polarization is adequately tuned. This is illustrated in Fig. 1 where we display the energy dependence of the mean longitudinal and transverse polarization of the top quark in the helicity system for different values of the effective polarization P_{eff} defined by

$$P_{\text{eff}} = \frac{h_- - h_+}{1 - h_- h_+}. \tag{1}$$

In Eq. (1), h_- and h_+ are the longitudinal polarization of the electron and positron beams, respectively. Note that, for unpolarized positron beams $h_+ = 0$, one has $P_{\text{eff}} = h_-$. For a given value of h_-, even small values of positron polarization of opposite sign will enhance the effective beam polarization. We shall return to this point in Sec. II. As compared to the work of Ref. [3], Fig. 1 now includes the $O(\alpha_s)$ radiative corrections. Large single-spin polarization effects due to beam polarization effects are also implicit in the work of Parke and Shadmi [5]. Although Ref. [5] is designed for the analysis of top-antitop quark spin correlations, it is easily adapted to single-spin polarization effects as also discussed in Ref. [6].

We shall see that the polarization of the top quark is governed by three parameters: the velocity $v = \sqrt{1 - 4m^2/s}$, the effective polarization P_{eff}, and the cosine of the scattering angle $\cos\theta$. At the respective boundaries of the three parameters the description of the polarization phenomena becomes reasonably simple, in particular, at the Born term level. The limits $v = 0$ (threshold) and $v = 1$ (high-energy limit) are discussed in Sec. IV. In Sec. V we discuss the limiting cases $P_{\text{eff}} = \pm 1$.

The two respective limiting cases $v = 0$, 1 and $P_{\text{eff}} = \pm 1$ contain in a nutshell much of the information that we want to discuss in the remaining part of the paper for intermediate values of these parameters. Many of the
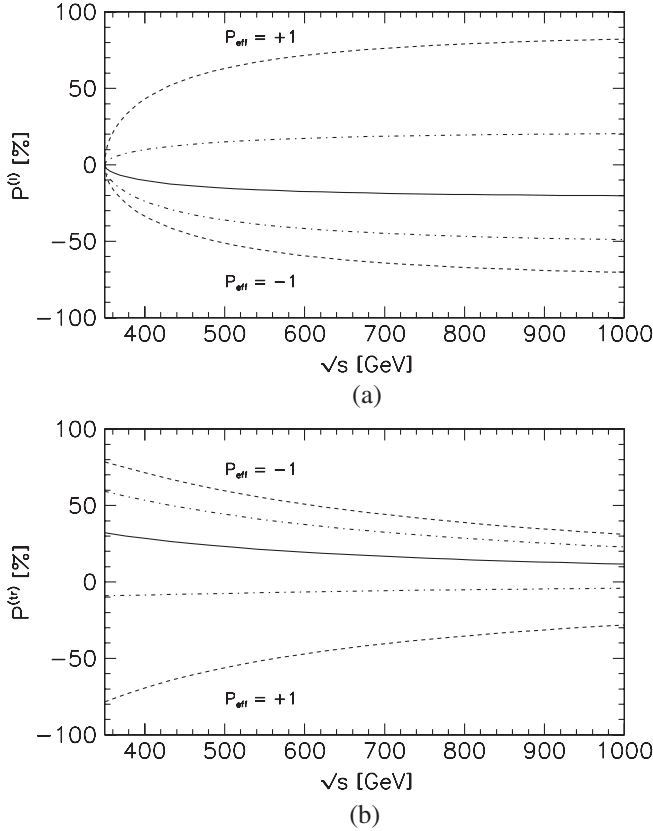
FIG. 1. Average (a) longitudinal polarization $\langle P^{(l)} \rangle$ and (b) transverse polarization $\langle P^{(\text{tr})} \rangle$ as a function of the c.m. energy $\sqrt{s}$, for the values $P_{\text{eff}} = -1$ (dashed), $P_{\text{eff}} = -0.5$ (dash-dotted), $P_{\text{eff}} = 0$ (solid), $P_{\text{eff}} = +0.5$ (dash-dotted), and $P_{\text{eff}} = +1$ (dashed). Averaging is over $\cos\theta$.

qualitative features of our results can be understood from extrapolations away from the two respective limits.

We shall also address the question of how to maximize and minimize the polarization of the top quark by tuning the beam polarization. Whereas a maximum polarization is optimal for the experimental determination of polarization effects, it is often desirable to gauge the quality of a polarization measurement against the corresponding unpolarized decay analysis. For some measurements it may even be advantageous to eliminate polarization effects altogether.

Of course, in the tuning process one has to bear in mind to keep the production rate at an acceptable level. This problem is not unrelated to the one of the original motivations of including beam polarization in linear colliders, namely, the gain in rate through beam polarization effects. We shall also address this question.

Our paper is structured as follows. In Sec. II we present the spin formalism of polarized beam production of top-antitop quark pairs including the polar angle dependence of the various spin components and longitudinal beam polarization effects. We present Born term and loop formulas for the relevant structure functions and collect general

expressions necessary for the numerators and the denominator of the polarization observables. Section III contains numerical next-to-leading (NLO) results on the angle-integrated rate and on polar angle distributions of the rate including beam polarization effects. We also provide numerical results on the left-right polarization asymmetry A_{LR}. In Sec. IV we discuss the limiting cases $\nu = 0$ and $\nu = 1$ at the Born term level. In Sec. V we describe the simplifications that occur for maximal effective beam polarizations $P_{\text{eff}} = \mp 1$ which correspond to the $(e^-_{L/R}, e^+_{R/L})$ beam configurations. In Sec. VI we discuss beam polarization effects on the three components of the top quark polarization vector. Section VII contains a discussion of the magnitude and the orientation of the polarization vector of the top quark. In Sec. VIII we present numerical NLO results on beam polarization effects on longitudinal spin-spin correlations of the top and antitop quark. Finally, Sec. IX contains a summary of our results and our conclusions. In an Appendix we list the electroweak coupling coefficients used in this paper and relate them to the chiral electroweak coupling coefficients used e.g. in Ref. [5].

Many of the quantitative arguments presented in this paper are based on Born term level results for which we give explicit alpha-numerical expressions for $\sqrt{s} = 500$ GeV. We emphasize, though, that all numerical results presented in the plots include the full $O(\alpha_s)$ radiative corrections where we have integrated over the full gluon phase space. By comparing the graphical NLO results with the numerical LO results, one can assess the size of the $O(\alpha_s)$ radiative corrections, at least for the representative energy of $\sqrt{s} = 500$ GeV. In general, the $O(\alpha_s)$ corrections to polarization observables are small (up to several percent) but can become much larger in some areas of phase space. A case in point is the longitudinal polarization of the bottom quark produced on the Z^0 at the backward point which obtains a 25% $O(\alpha_s)$ correction when $P_{\text{eff}} = +1$ [4]. As we shall see later on, the $O(\alpha_s)$ corrections to $(t\bar{t})$ production can amount up to 12% (see Sec. VII). In addition, there are polarization observables that are zero at the Born term level and become populated only at $O(\alpha_s)$. Among these are the normal component of the polarization (see Sec. VI) and the longitudinal polarization produced from a longitudinal intermediate vector boson (see Sec. II).

II. SPIN FORMALISM OF POLARIZED BEAM PRODUCTION

The production of top quark pairs at a linear e^+e^- collider proceeds via γ and Z exchange:

$$e^- e^+ \overset{\gamma, Z}{\rightarrow} t\bar{t}. \tag{2}$$

At the center of mass energies which are being envisaged at the ILC ($s = (p_{e^-} + p_{e^+})^2$), $\sqrt{s} \sim 2m_t \div 1000$ GeV, top quark pairs will be produced with nonrelativistic velocities

in the threshold region ($v \to 0$) up to relativistic velocities of $v = 0.937$ at the highest energy $\sqrt{s} = 1000$ GeV ($v = \sqrt{1 - 4m_t^2/s}$).[1] This enables the study of the complete production phenomena with different polarization and correlation effects that reach from the nonrelativistic to the relativistic domain. For unpolarized beams the total rate is dominated by the diagonal ($\gamma - \gamma$) and the ($Z - Z$) rates which contribute at the same order of magnitude. The ($\gamma - Z$) interference contribution to the total rate is suppressed due to the smallness of the vector (Ze^+e^-) coupling v_l ($v_l = -1 + 4\sin^2\theta_W$). The ($\gamma - Z$) interference contribution can, however, become quite sizable for polarized beams, for the polar angle dependent rates, and for top quark polarization effects.

We mention that, at threshold, there will be the opportunity for very precise measurements of the top quark mass and width, as well as of the strong coupling α_s. In this region, perturbative QCD is no longer applicable. One has to solve the Schrödinger equation for the relevant Green functions in a nonrelativistic approximation for a Coulombic potential, i.e. the nonrelativistic QCD method, described first in Ref. [8] and later applied to the calculation of various different quantities at threshold (see, for example, the discussion in Refs. [9,10] and references therein). In this paper we shall discuss top-antitop production well above threshold where perturbation theory can be safely applied. For our purposes we take the perturbative regime to start approximately 10 GeV above threshold. Throughout this paper we shall take the top quark mass to have a nominal value of 175 GeV. Therefore, we shall consider c.m. beam energies starting from $\sqrt{s} = 360$ GeV.

We are going to discuss the most general case of the polarization of the top quark with arbitrary longitudinal polarizations of the e^- and e^+ beams. The rate depends on the set of four parameters $\{h_- \in [-1, 1], h_+ \in [-1, 1], v \in [0, 1], \cos\theta \in [-1, 1]\}$ or, equivalently, on the set $\{K_G \in [0, 2], P_{\text{eff}} \in [-1, 1], v \in [0, 1], \cos\theta \in [-1, 1]\}$, where we shall call $K_G = 1 - h_-h_+$ the gain factor. We have indicated the range of the parameter values in square brackets. In contrast to the rate, the polarization of the top quark depends only on the set of the three parameters $\{P_{\text{eff}}, v, \cos\theta\}$. When discussing our predictions we shall attempt to explore the whole four- and three-dimensional parameter space for the rate and polarization, respectively. We mention that the beam polarizations envisaged at the ILC are $h_- = \pm 90\%$ for electrons and $h_+ = \pm 80\%$ for positrons [11].

We will see that beam polarizations significantly influence the polarization phenomena of a top quark. In addition, adequately tuned beam polarization can enhance the top-antitop quark signal and suppress other background processes such as W-pair production (see discussion in Ref. [12]).

In what follows, we concentrate on the polarization of the top quark, i.e. we sum over the polarization of the antitop quark. The polarization of the antitop quark can be obtained from the corresponding polarization components of the top quark using CP invariance as will be discussed in the summary section. Even more structure is revealed when one considers joint top-antitop polarization. In order to reveal this structure, one must perform a joint analysis of the decay products of the top and antitop quark. ($t\bar{t}$) spin-spin correlations will be briefly discussed in Sec. VIII at the end of the paper.

The general expression of the cross section for ($t\bar{t}$) production in e^+e^- collisions is given by[2]

$$d\sigma^{(m)} = 2\pi\frac{e^4}{s^2}\sum_{i,j=1}^{4} g_{ij}L^{i\mu\nu}H_{\mu\nu}^{j(m)}dPS. \quad (3)$$

$L_{\mu\nu}^i$ is the lepton tensor, $H_{\mu\nu}^j$ is the hadron tensor encoding the hadronic production dynamics, dPS is the phase space factor, and the g_{ij} are the elements of the electroweak coupling matrix which are defined in the Appendix. The sum runs over the four independent configurations of products of the vector and axial vector currents, i.e. $i, j = 1, 2$ for $(VV \pm AA)/2$, $i, j = 3$ for $i(VA - AV)/2$, and $i, j = 4$ for $(VA + AV)/2$ for the product of lepton and quark currents, and m denotes one of the possible polarization configurations of the top quark: longitudinal ($m = \ell$), transverse ($m = $ tr) in the beam scattering plane and normal ($m = n$) to the beam scattering plane. Our choice of the three orthonormal spin directions ($\vec{e}^{(\text{tr})}, \vec{e}^{(n)}, \vec{e}^{(\ell)}$) are given by

$$\vec{e}^{(\text{tr})} = \frac{(\vec{p}_{e^-} \times \vec{p}_t) \times \vec{p}_t}{|(\vec{p}_{e^-} \times \vec{p}_t) \times \vec{p}_t|},$$

$$\vec{e}^{(n)} = \frac{\vec{p}_{e^-} \times \vec{p}_t}{|\vec{p}_{e^-} \times \vec{p}_t|}, \quad (4)$$

$$\vec{e}^{(\ell)} = \frac{\vec{p}_t}{|\vec{p}_t|}.$$

In Fig. 2 we have drawn the directions of $\vec{e}^{(\text{tr})}$ and $\vec{e}^{(\ell)}$ for a generic top quark direction; the vector $\vec{e}^{(n)}$ shows out of the plane. For the unpolarized top quark case the superscript (m) is dropped in Eq. (3). The explicit definitions for all the above quantities together with explicit analytical expressions for the radiative corrections can be found in Refs. [14,19–21] (see also Ref. [4]).

---

[1] In the first stage of the ILC, one will reach energies up to 500 GeV with an optional second stage upgrade to 1000 GeV [1,2]. For the multi-TeV collider CLIC, one foresees energies up to 3 TeV [7].

[2] The spin kinematics of e^+e^- collisions has been formulated in a number of papers. These include the unpublished DESY report [13] of which the portions relevant to this paper have been summarized in Ref. [14]. Other papers on the subject are Refs. [4,12,15–18].

We proceed with the discussion in the helicity basis, i.e. we take the direction of the top quark to define the z direction of the hadronic system. For unpolarized beams the angular decomposition of the differential polarized cross section can be written as

$$\frac{d\sigma^{(m)}}{d\cos\theta} = \frac{3}{8}(1 + \cos^2\theta)\sigma_U^{(\ell)} + \frac{3}{4}\sin^2\theta\sigma_L^{(\ell)} + \frac{3}{4}\cos\theta\sigma_F^{(\ell)}$$
$$- \frac{3}{\sqrt{2}}\sin\theta\cos\theta\sigma_I^{(\mathrm{tr},n)} - \frac{3}{\sqrt{2}}\sin\theta\sigma_A^{(\mathrm{tr},n)}, \quad (5)$$

where, at NLO of QCD,

$$\sigma_a^{(m)} = \frac{\pi\alpha^2 v}{3s^2}\sum_{j=1}^{4} g_{1j}(H_a^{j(m)}(\mathrm{Born}) + H_a^{j(m)}(\alpha_s))$$

for $a = U, L, I$ (6)

and

$$\sigma_a^{(m)} = \frac{\pi\alpha^2 v}{3s^2}\sum_{j=1}^{4} g_{4j}(H_a^{4(m)}(\mathrm{Born}) + H_a^{4(m)}(\alpha_s))$$

for $a = F, A$. (7)

In Eq. (5) we have rewritten the covariant representation (3) in terms of helicity structure functions $\sigma_a^{(m)}$. The angle θ is the polar angle between the momentum of the top quark and the electron momentum (see Fig. 2). For example, in the purely electromagnetic case $e^+e^- \to \gamma^* \to q\bar{q}$, one obtains the LO formula

$$\frac{d\sigma}{\cos\theta} = 2\pi N_c Q_f^2 v \frac{\alpha^2}{4s}(1 + \cos^2\theta + (1 - v^2)\sin^2\theta) \quad (8)$$

using the LO born term expressions listed later in Eq. (10). The distribution (8) agrees with Eq. (41.2) in the Particle Data Group booklet. We mention that our $O(\alpha_s)$ corrections agree with those in Ref. [4] after correcting a sign mistake in the normal polarization (see Erratum in Ref. [21]).
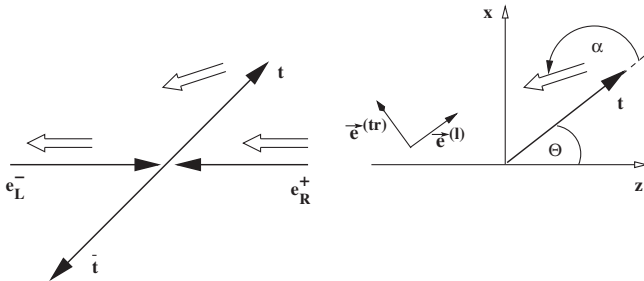

FIG. 2. A generic configuration for top pair production and top polarization at a polarized e^+e^- collider with a (e_L^-, e_R^+) polarization. The positive z axis points into the direction of the electron momentum. The angle α is the polar angle of the top quark polarization relative to the top quark momentum measured anticlockwise from the direction of the top quark.

Above the top quark threshold, one is sufficiently far away from the Z-boson pole to neglect the imaginary part of the Z boson pole propagator. This can be appreciated from the Breit-Wigner line shape of the Z propagator, viz.

$$\chi_Z = \frac{1}{s - M_Z^2 + iM_Z\Gamma_Z}$$
$$= \frac{1}{s - M_Z^2}\left(1 - i\frac{M_Z\Gamma_Z}{s - M_Z^2}\right)\Big/\left(1 + \frac{M_Z^2\Gamma_Z^2}{(s - M_Z^2)^2}\right). \quad (9)$$

The factor $M_Z\Gamma_Z/(s - M_Z^2)$ determines the ratio of the imaginary and real parts of the Z propagator $\mathrm{Im}\chi_Z/\mathrm{Re}\chi_Z$. It is already quite small at threshold (~ 0.002) and falls off with s^{-1}. Dropping the imaginary part contribution of the Z propagator implies that we neglect contributions proportional to g_{13} in Eq. (6) and g_{43} in Eq. (7). We shall also neglect the width dependence in the real part of the Z propagator because it is negligibly small.

The nonvanishing unpolarized Born term contributions $H_a^j(\mathrm{Born})$ read

$$H_U^1(\mathrm{Born}) = 2N_c s(1 + v^2),$$
$$H_L^1(\mathrm{Born}) = N_c s(1 - v^2) = H_L^2(\mathrm{Born}),$$
$$H_U^2(\mathrm{Born}) = 2N_c s(1 - v^2),$$
$$H_F^4(\mathrm{Born}) = 4N_c s v. \quad (10)$$

One has $(1 - v^2) = 4m_t^2/s$ showing that the longitudinal rate H_L falls off with a s^{-1} power behavior relative to the transverse rates $H_{U,F}$. The longitudinally polarized contributions read

$$H_U^{4(\ell)}(\mathrm{Born}) = 4N_c s v,$$
$$H_F^{1(\ell)}(\mathrm{Born}) = 2N_c s(1 + v^2),$$
$$H_L^{4(\ell)}(\mathrm{Born}) = 0,$$
$$H_F^{2(\ell)}(\mathrm{Born}) = 2N_c s(1 - v^2). \quad (11)$$

Note that one has the Born term relations

$$H_U^{4(\ell)}(\mathrm{Born}) = H_F^4(\mathrm{Born}),$$
$$H_F^{1,2(\ell)}(\mathrm{Born}) = H_U^{1,2}(\mathrm{Born}), \quad (12)$$

which are due to angular momentum conversation in the back-to-back configuration at the Born term level. It is quite clear that Eqs. (12) no longer hold true in general at $O(\alpha_s)$ since quark and antiquark are no longer back to back in general due to additional gluon emission. The relations (12) will be useful in our subsequent discussion of the longitudinal polarization at the forward and backward points. Notable also is the relation $H_L^{4(\ell)}(\mathrm{Born}) = 0$ in Eq. (11) which is again related to the LO back-to-back configuration. The radiative corrections to the corresponding polarization component $P_L^{(\ell)}$ have been studied in

Ref. [20] and have been found to be small of $O(0.1\%)$ when averaged over gluon phase space. For small top quark energies $P_L^{(\ell)}$ can become as large as 3% at $\sqrt{s} = 500$ GeV.

For the transverse polarization components, one has [21]

$$
\begin{aligned}
H_I^{4(\mathrm{tr})}(\text{Born}) &= 2N_c s v \frac{m_t}{\sqrt{2s}}, \\
H_A^{1(\mathrm{tr})}(\text{Born}) &= 2N_c s \frac{m_t}{\sqrt{2s}} = H_A^{2(\mathrm{tr})}(\text{Born}).
\end{aligned}
\tag{13}
$$

The only nonnegligible contribution to the normal polarization component $P^{(n)}$ comes from the imaginary part of the one-loop contribution ($C_F = 4/3$)

$$
H_I^{1(n)}(\text{loop}) = 2N_c s \frac{\alpha_s C_F}{4\pi} \pi v \frac{m_t}{\sqrt{2s}} = H_I^{2(n)}(\text{loop}), \tag{14}
$$

$$
H_A^{4(n)}(\text{loop}) = 2N_c s \frac{\alpha_s C_F}{4\pi} \pi (2 - v^2) \frac{m_t}{\sqrt{2s}}. \tag{15}
$$

As already mentioned in the Introduction, the transverse and normal polarization components can be seen to fall off with a power behavior of $(\sqrt{s})^{-1}$ relative to the longitudinal polarization components.

The α_s corrections to the polarized structure functions $H_a^{j(m)} = H_a^j(+s^m) - H_a^j(-s^m)$ and the unpolarized structure function $H_a^j = H_a(+s^m) + H_a(-s^m)$ (s^m is the polarization vector of the top quark) are too lengthy to be listed here. They can be found in Refs. [14,19–21], or, in a very compact two-page analytical representation, in Sec. 5 of Ref. [22].

The longitudinal polarization of the electron and positron beams enter the above formulas as [14][3]

$$
\begin{aligned}
g_{1j} &\to (1 - h_- h_+) g_{1j} + (h_- - h_+) g_{4j} \\
&= (1 - h_- h_+)(g_{1j} + P_{\mathrm{eff}} g_{4j}), \\
g_{4j} &\to (1 - h_- h_+) g_{4j} + (h_- - h_+) g_{1j} \\
&= (1 - h_- h_+)(g_{4j} + P_{\mathrm{eff}} g_{1j}),
\end{aligned}
\tag{16}
$$

where P_{eff} is defined in Eq. (1). In Eq. (16) h_- denotes the electron's and h_+ denotes the positron's longitudinal polarization which can take values between ± 1. An electron with $h_- = \mp 1$ will be referred to as the totally polarized left-handed (right-handed) electron ($e_{L/R}^-$). Similarly, a right-handed positron (e_R^+) has $h_+ = -1$ and a left-handed positron (e_L^+) has $h_+ = +1$. From the definition of P_{eff} [see Eq. (1)] it is clear that large values of P_{eff} can be reached even for nonmaximal values of h_- and h_+, as Fig. 3(a) shows. For example, the large value of $P_{\mathrm{eff}} = -0.95$ can be achieved with $h_- = -0.8$; $h_+ = 0.625$,

and correspondingly, $P_{\mathrm{eff}} = 0.95$ can be reached with $h_- = 0.8$; $h_+ = -0.625$. These two examples have been marked off in Fig. 3. Both sets correspond to a gain factor of $K_G = 1.5$.
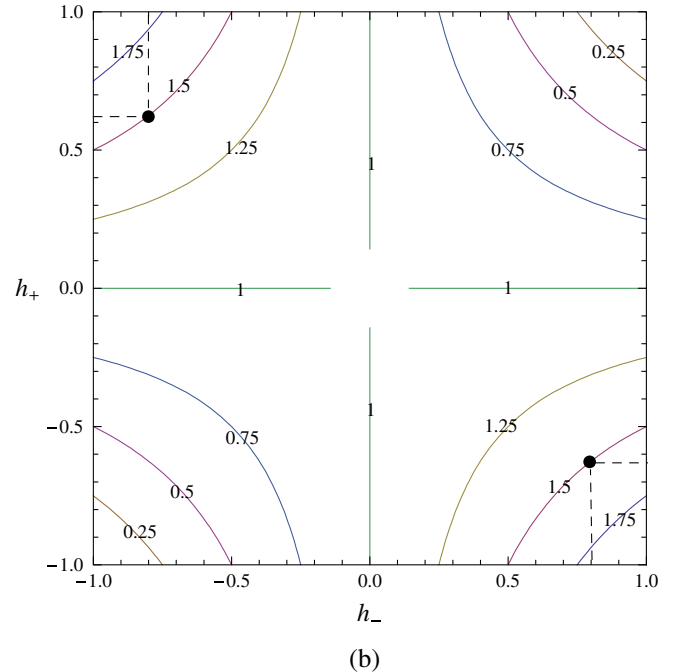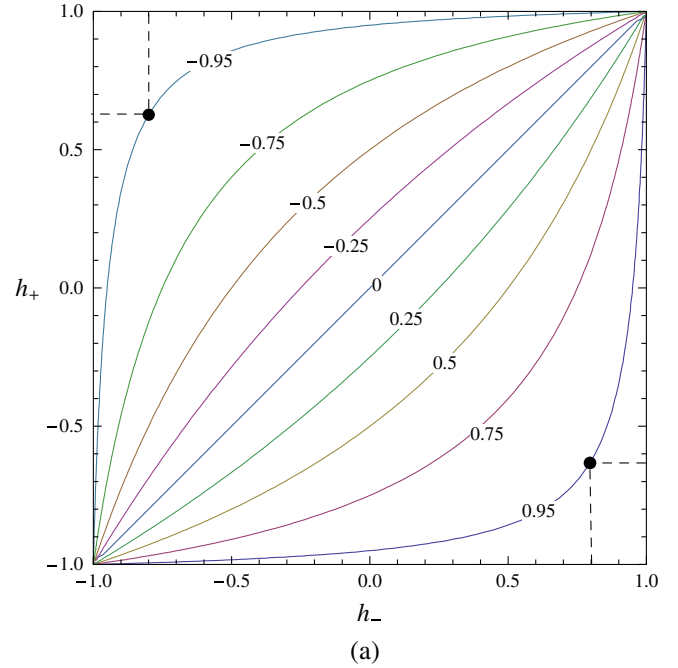

(a)

(b)

FIG. 3 (color online). Contour plots in the (h_-, h_+) plane (a) for fixed values of the effective polarization $P_{\mathrm{eff}} = (h_- - h_+)/(1 - h_- h_+)$ and (b) for fixed values of the gain factor $K_G = (1 - h_- h_+)$. The two points marked off in the plots correspond to $(h_-, h_+) = (-0.8, +0.625)$ and $(+0.8, -0.625)$, respectively.

---

[3]Transverse beam polarization effects will not be discussed in this paper because present plans call for longitudinal beam polarization at the ILC. Transverse beam polarization effects can be included as described e.g. in Ref. [14].

The orientation-dependent longitudinal, transverse, and normal polarization components which we are interested in are defined by

$$P^{(m)}(\cos\theta) = \frac{d\sigma^{(m)}/d\cos\theta}{d\sigma/d\cos\theta} \qquad m = \ell, tr, n, \qquad (17)$$

where $d\sigma/d\cos\theta$ is the unpolarized differential cross section. Of course, there is an additional dependence of the above quantities on the c.m. beam energy $\sqrt{s}$, and on the beam polarizations h_- and h_+ to be discussed later on. The unpolarized cross section is given by the first three terms in Eq. (5) dropping, of course, the label (ℓ).

Dropping the common factor $\pi\alpha^2 v/(3s^2)$ in the ratio (17), we shall represent the polarization components by the ratios

$$P^{(m)}(\cos\theta) = \frac{N^{(m)}(\cos\theta)}{D(\cos\theta)}, \qquad m = \ell, tr, n. \qquad (18)$$

In particular, the gain factor K_G has canceled out in the ratio (18) implying that the polarization only depends on P_{eff}.

The numerator factors $N^{(m)}$ in Eq. (18) are given by

$$
\begin{aligned}
N^{(\ell)}(\cos\theta) = &\tfrac{3}{8}(1 + \cos^2\theta)(g_{14} + g_{44}P_{\text{eff}})H_U^{4(\ell)} \\
&+ \tfrac{3}{4}\sin^2\theta(g_{14} + g_{44}P_{\text{eff}})H_L^{4(\ell)} \\
&+ \tfrac{3}{4}\cos\theta((g_{41} + g_{11}P_{\text{eff}})H_F^{1(\ell)} \\
&+ (g_{42} + g_{12}P_{\text{eff}})H_F^{2(\ell)}), \qquad (19)
\end{aligned}
$$

$$
\begin{aligned}
N^{(\text{tr})}(\cos\theta) = &-\frac{3}{\sqrt{2}}\sin\theta\cos\theta(g_{14} + g_{44}P_{\text{eff}})H_I^{4(\text{tr})} \\
&- \frac{3}{\sqrt{2}}\sin\theta((g_{41} + g_{11}P_{\text{eff}})H_A^{1(\text{tr})} \\
&+ (g_{42} + g_{12}P_{\text{eff}})H_A^{2(\text{tr})}), \qquad (20)
\end{aligned}
$$

and by

$$
\begin{aligned}
N^{(n)}(\cos\theta) = &-\frac{3}{\sqrt{2}}\sin\theta\cos\theta((g_{11} + g_{41}P_{\text{eff}})H_I^{1(n)}(\text{loop}) \\
&+ (g_{12} + g_{42}P_{\text{eff}})H_I^{2(n)}(\text{loop})) \\
&- \frac{3}{\sqrt{2}}\sin\theta(g_{44} + g_{14}P_{\text{eff}})H_A^{4(n)}(\text{loop}). \qquad (21)
\end{aligned}
$$

For the denominator, one has

$$
\begin{aligned}
D(\cos\theta) = &\tfrac{3}{8}(1 + \cos^2\theta)((g_{11} + g_{41}P_{\text{eff}})H_U^1 \\
&+ (g_{12} + g_{42}P_{\text{eff}})H_U^2) + \tfrac{3}{4}\sin^2\theta((g_{11} + g_{41}P_{\text{eff}})H_L^1 \\
&+ (g_{12} + g_{42}P_{\text{eff}})H_L^2) + \tfrac{3}{4}\cos\theta(g_{44} + g_{14}P_{\text{eff}})H_F^4.
\end{aligned}
$$
$$(22)$$

At the forward (FP) and backward (BP) point the transverse and normal polarization components vanish. Referring to the relations (12), at Born term level the longitudinal polarization component $P^{(\ell)}$ takes a very simple form at the forward (FP) and backward (BP) point for the maximal values of the effective polarization $P_{\text{eff}} = \pm 1$. One has

$$
\begin{aligned}
\text{FP:}\ &P^{(\ell)}(\cos\theta = +1) = \pm 1, \\
\text{BP:}\ &P^{(\ell)}(\cos\theta = -1) = \mp 1,
\end{aligned}
\qquad (23)
$$

in agreement with angular momentum conservation. It is clear that these relations no longer hold true in general at NLO due to hard gluon emission.

It is useful to define the left-right polarization asymmetry A_{LR} through the relation

$$\frac{d\sigma(P_{\text{eff}}) - d\sigma(-P_{\text{eff}})}{d\sigma(P_{\text{eff}}) + d\sigma(-P_{\text{eff}})} = -A_{LR}P_{\text{eff}}, \qquad (24)$$

where

$$A_{LR} = -\frac{\tfrac{3}{8}(1 + \cos^2\theta)(g_{41}H_U^1 + g_{42}H_U^2) + \tfrac{3}{4}\sin^2\theta(g_{41}H_L^1 + g_{42}H_L^2) + \tfrac{3}{4}\cos\theta g_{14}H_F^4}{\tfrac{3}{8}(1 + \cos^2\theta)(g_{11}H_U^1 + g_{12}H_U^2) + \tfrac{3}{4}\sin^2\theta(g_{11}H_L^1 + g_{12}H_L^2) + \tfrac{3}{4}\cos\theta g_{44}H_F^4}. \qquad (25)$$

Of interest is the angle α enclosed by the momentum and the polarization of the top quark projected onto the scattering plane (see Fig. 2).[4] The angle α is determined by

$$\tan\alpha(\cos\theta) = \frac{N^{(\text{tr})}(\cos\theta)}{N^{(\ell)}(\cos\theta)}. \qquad (26)$$

---

[4] For the present purposes we neglect the $O(\alpha_s)$ normal component of the polarization vector which is quite small. Note that, in general, one needs two angles to describe the orientation of the polarization vector instead of the one angle α defined in Eq. (26).

Equation (26) assumes a simple form at threshold and in the high-energy limit as discussed in Sec. IV, and for $P_{\text{eff}} = \pm 1$ as will be discussed in Sec. V. The correlations between α and θ implied by Eq. (26) will be discussed in Secs. IV, V, and VII.

III. BEAM POLARIZATION DEPENDENCE OF THE RATE

We begin our numerical discussion with the rate proportional to the denominator expression in Eq. (18). The effect of longitudinally polarized beams on the polar averaged rate (called total rate) can be obtained from the form

$$\sigma = \sigma(P_{\text{eff}} = 0)(1 - h_- h_+)\left(1 + P_{\text{eff}}\frac{g_{41}}{g_{11}}\frac{1 + \frac{g_{42}}{g_{41}}\frac{H^2_{U+L}}{H^1_{U+L}}}{1 + \frac{g_{12}}{g_{11}}\frac{H^2_{U+L}}{H^1_{U+L}}}\right),$$

$$(27)$$

which, at the Born level and at $\sqrt{s} = 500$ GeV, gives

$$\sigma = \sigma(P_{\text{eff}} = 0)(1 - h_- h_+)(1 - 0.37 P_{\text{eff}}). \qquad (28)$$

From Eq. (28) it is evident that the total rate becomes maximal on two counts: (i) large values of the gain factor $K_G = (1 - h_- h_+)$, requiring $\text{sign}(h_-) = -\text{sign}(h_+)$; and (ii) large negative values of P_{eff}, which can be achieved with large negative and positive values of h_- and h_+, respectively. The maximal enhancement of the rate will be obtained for $h_- = -1$ and $h_+ = +1$ such that $P_{\text{eff}} = -1$ and $K_G = 2$. At $\sqrt{s} = 500$ GeV, this leads to a maximal enhancement factor of 2.74 over the unpolarized case. It is interesting to note that for $(b\bar{b})$ production at $\sqrt{s} = 500$ GeV the effective enhancement through beam polarization effects is slightly larger than in the $(t\bar{t})$ case. For $(b\bar{b})$ production the last factor in Eq. (27) is replaced by the simpler expression $(1 + P_{\text{eff}} g_{41}/g_{11})$ since, at $\sqrt{s} = 500$ GeV, the ratio H^2_{U+L}/H^1_{U+L} is practically zero for bottom quark production. Using the results of the Appendix applied to the $(b\bar{b})$ case, one finds $g_{41}/g_{11} = -0.62$ leading to an overall enhancement factor of 3.24 for the optimal choice of parameters $h_- = -1$ and $h_+ = +1$ $(P_{\text{eff}} = -1)$ at $\sqrt{s} = 500$ GeV.

In Fig. 3(b) we show some contour lines for fixed values of the gain factor $K_G = (1 - h_- h_+)$ in the (h_-, h_+) plane. Clearly, quadrants 2 and 4 are favored if one wants to obtain a gain factor exceeding one, i.e. $K_G \geq 1$. As concerns the rate dependence on P_{eff} [rightmost factor in Eq. (28)], a further rate enhancement is achieved for negative values of P_{eff}, i.e. one would have to choose points lying to the left of the line $h_- = -h_+$ in Fig. 3(a). The optimal choice as concerns the rate would thus be quadrant 2 in the (h_-, h_+) plane. One notes that large negative values of P_{eff} can readily be achieved for nonmaximal values of the beam polarization, as illustrated in Fig. 3(a), where we have plotted some contour lines in the (h_-, h_+) plane corresponding to fixed values of P_{eff}. One notes that the regions of large K_G and large negative P_{eff} have a large overlap. We mention that one may have to give up the optimal choice in the (h_-, h_+) plane if one wants to achieve other goals such as minimizing the polarization.

The QCD one-loop corrections to the total cross section are well known (see e.g. Ref. [18]) and add about 13% at $\sqrt{s} = 500$ GeV to the Born total cross section, where the percentage increase has very little dependence on the beam polarization. We mention that the electroweak corrections to the total rate are smaller, and amount to about 50% of the QCD corrections [23]. For the strong coupling α_s we use two-loop running adjusted to the value $\alpha_s(m_Z) = 0.1175$
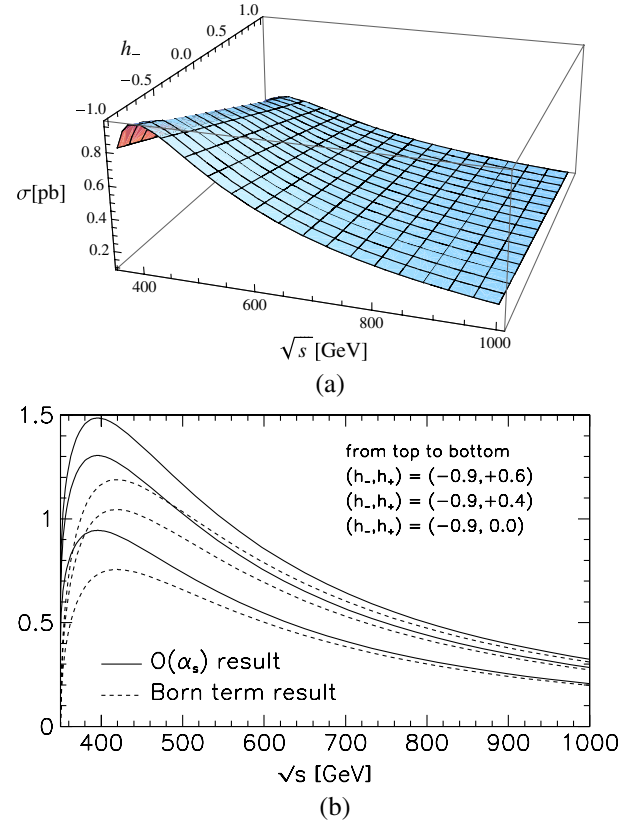

(a)

(b)

FIG. 4 (color online). The total cross section σ at the one-loop level as a function of the beam energy $\sqrt{s}$ and (a) the electron polarization h_- ($h_+ = 0$); (b) for three values of the positron polarization $h_+ = 0$, 0.4, 0.6, and with the fixed electron beam polarization of $h_- = -0.9$ (solid lines). In Fig. 4(b) we also show the respective LO rates (dashed lines).

and fitted at $2m_t = 350$ GeV.[5] Close to threshold the $O(\alpha_s)$ corrections become larger and amount to about 27% of the total cross section at e.g. $\sqrt{s} = 400$ GeV. The c.m. energy dependence of the total cross section σ is shown in Figs. 4(a) and 4(b). In Fig. 4(a) we take $h_+ = 0$ and show the energy dependence of the total cross section varying h_- over its whole range $[-1, +1]$. One notes a strong dependence on h_- apart from the standard falloff of the total cross section with beam energy. Since for $h_+ = 0$ the gain factor K_G is equal to 1 and since $P_{\text{eff}} = h_-$, the rate depends linearly on h_- as displayed in Eqs. (27) and (28). The rate is largest for $h_- = -1$ and then linearly drops to its lowest value at $h_- = +1$. In Fig. 4(b) we show the energy dependence of the rate for the three pairs of beam polarizations $(h_-, h_+) = (-0.9, 0)$, $(-0.9, +0.4)$, $(-0.9, +0.6)$. If one translates this into the (K_G, P_{eff}) representation, one has $(K_G, P_{\text{eff}}) = (1, -0.9)$, $(1.36, -0.96)$, $(1.54, -0.97)$. The hierarchy of

_____

[5]For α we take the value $\alpha = 1/137$. If one uses a running α, for example $\alpha = 1/128$, the cross sections in Fig. 4 would increase by 14.6%.

rates in Fig. 4(b) can be seen to be mostly determined by the gain factor K_G in Eq. (27).

Next we turn to the differential rate distribution with respect to $\cos\theta$. In order to illustrate the forward dominance of the differential $\cos\theta$ distribution we plot $\sigma^{-1}d\sigma/d\cos\theta$ against $\cos\theta$. Note that the dependence on the gain factor $K_G = 1 - h_- h_+$ drops out in the ratio. In Fig. 5(a) we plot the differential rate distribution for a fixed value of $\sqrt{s} = 500$ GeV and for $P_{\text{eff}} = -1, 0, +1$. One sees a pronounced forward dominance of the differential distribution which does not depend much on the value of P_{eff}. In Fig. 5(b) we keep the effective beam polarization fixed at $P_{\text{eff}} = 0$ and vary $\sqrt{s}$ through several values. At threshold $\sqrt{s} = 350$ GeV, one has a flat distribution $\sigma^{-1}d\sigma/d\cos\theta = 0.5$. When the energy is increased, the forward rate clearly dominates over the backward rate. The forward dominance becomes even stronger for increasing energies.

Of related interest is the rate into the forward (F) and backward (B) hemispheres. Again, the gain factor K_G drops out in the ratio. At $\sqrt{s} = 500$ GeV, one numerically obtains
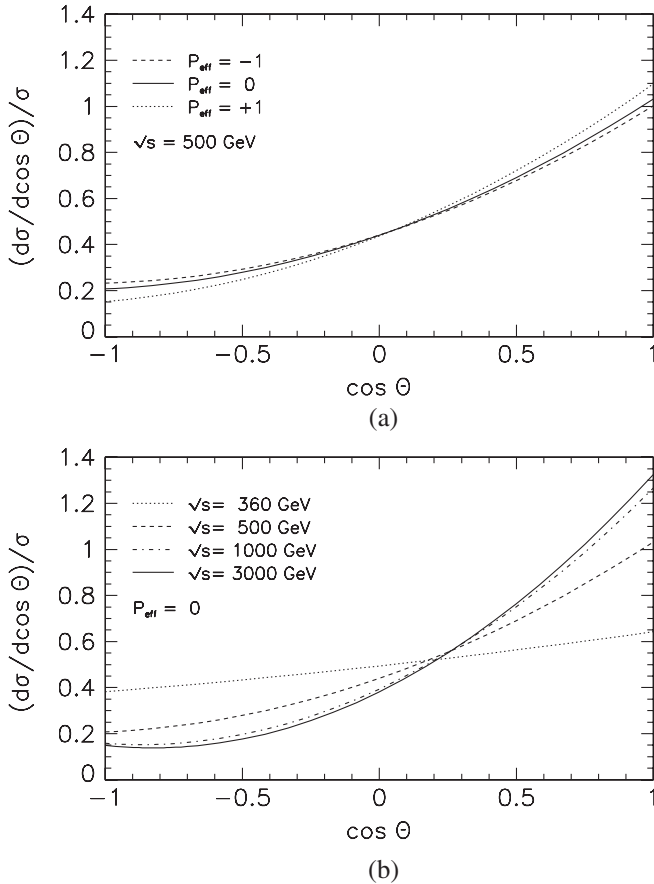

(a)

(b)

FIG. 5. Polar angle dependence of the differential cross section for (a) $\sqrt{s} = 500$ GeV and $P_{\text{eff}} = -1, 0, +1$ and (b) $P_{\text{eff}} = 0$ for beam energies $\sqrt{s} = 360$ GeV (dotted line), 500 GeV (dashed line), 1000 GeV (dash-dotted line), and 3000 GeV (solid line).
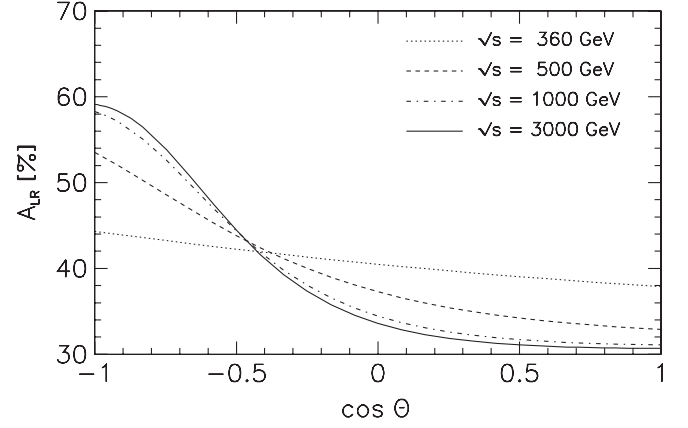

FIG. 6. Left-right polarization asymmetry A_{LR} for $\sqrt{s} = 360$, 500, 1000, and 3000 GeV (notation as in Fig. 5).

$$\frac{\langle\sigma\rangle_F}{\langle\sigma\rangle_B} = \frac{\langle\sigma\rangle_F}{\langle\sigma\rangle_B}\bigg|_{P_{\text{eff}}=0} \frac{1 - 0.34P_{\text{eff}}}{1 - 0.43P_{\text{eff}}}$$
$$= \left\{\begin{array}{ll} +2.73 & P_{\text{eff}} = +1 \\ +2.36 & = 0 \\ +2.21 & = -1 \end{array}\right\}. \qquad (29)$$

The mean forward rate $\langle\sigma\rangle_F$ clearly dominates over the mean backward rate $\langle\sigma\rangle_B$. The dependence of the F/B rate ratio on P_{eff} is not very pronounced.

In Fig. 6 we plot the polar angle dependence of the NLO left-right polarization asymmetry A_{LR} for different energies. At $\sqrt{s} = 360$ GeV the $\cos\theta$ dependence already starts to deviate from the flat Born term behavior at threshold given by $A_{LR} = -(g_{41} + g_{42})/(g_{11} + g_{12}) = 0.409$. The left-right polarization asymmetry A_{LR} peaks toward the backward region and reaches $\approx 59\%$ at the backward point for the highest energy $\sqrt{s} = 3000$ GeV in Fig. 6.

IV. BORN TERM SIMPLIFICATIONS AT THRESHOLD AND IN THE HIGH-ENERGY LIMIT

Before turning to the numerical analysis of the polarization of the top quark, in this section we shall first discuss Born term simplifications of the polarization of the top quark at threshold and in the high-energy limit. In Sec. V we discuss Born term simplifications that occur for $P_{\text{eff}} = \mp 1$.

At threshold $v \to 0$ and in the high-energy limit $v \to 1$, the polarization expressions become quite simple. At threshold, the polarization of the top quark is parallel to the beam axis, regardless of the polar orientation of the top quark (see e.g. Ref. [24]). In fact, a large part of the beam polarization gets transferred to the polarization of the top quark at threshold. For the Born term contributions the top quark polarization at threshold can be calculated from

Eqs. (19), (20), and (22) (see also Refs. [18,25]). It is nominally given by[6]

$$\vec{P} = \frac{P_{\mathrm{eff}} - A_{LR}}{1 - P_{\mathrm{eff}} A_{LR}} \hat{n}_{e^-}, \qquad (30)$$

where A_{LR} is the left-right beam polarization asymmetry $(\sigma_{LR} - \sigma_{RL})/(\sigma_{LR} + \sigma_{RL})$ at threshold [see Eq. (25)] and $\hat{n}_{e^-}$ is a unit vector pointing into the direction of the electron momentum. In terms of the electroweak coupling parameters g_{ij} (see the Appendix), the nominal polarization asymmetry at threshold $\sqrt{s} = 2m_t$ is given by $A_{LR} = -(g_{41} + g_{42})/(g_{11} + g_{12}) = 0.409$. The simplification at threshold arises from the fact that, from the four $(L, S)_{V,A}$ amplitudes $(L, S)_{V,A} = (0, 1)_V, (2, 1)_V, (1, 0)_A, (1, 1)_A$ describing the production of a spin-1/2 pair, only the S-wave amplitude $(0, 1)_V$ survives at threshold. The suffixes V and A denote vector current (V) and axial vector current (A) production. Correspondingly, the combinations $(g_{41} + g_{42})$ and $(g_{11} + g_{12})$ contain only the vector current coupling on the quark side.

The magnitude of the threshold polarization is given by

$$|\vec{P}| = \left| \frac{P_{\mathrm{eff}} - A_{LR}}{1 - P_{\mathrm{eff}} A_{LR}} \right|. \qquad (31)$$

The threshold polarization is independent of $\cos\theta$, i.e. $\langle|\vec{P}|\rangle = |\vec{P}|$. The polarization vanishes for $P_{\mathrm{eff}} = A_{LR}$ independent of $\cos\theta$.[7] For $P_{\mathrm{eff}} > A_{LR}$ and $P_{\mathrm{eff}} < A_{LR}$, one has $\vec{P} = |\vec{P}|\hat{n}_{e^-}$ and $\vec{P} = -|\vec{P}|\hat{n}_{e^-}$, respectively, such that $P^{(\mathrm{tr})} = \mp|\vec{P}| \sin\theta$ and $P^{(\ell)} = \pm|\vec{P}| \cos\theta$. In particular, one has a 100% threshold polarization of the top quark for $P_{\mathrm{eff}} = \pm 1$ with $\vec{P} = \pm\hat{n}_{e^-}$.

Extrapolations away from $P_{\mathrm{eff}} = \pm 1$ are more stable for $P_{\mathrm{eff}} = -1$ than for $P_{\mathrm{eff}} = +1$ as the slope of Eq. (31) at $P_{\mathrm{eff}} = \pm 1$ shows. One has

$$\frac{d|\vec{P}|}{dP_{\mathrm{eff}}} = \pm \frac{1 \pm A_{LR}}{1 \mp A_{LR}}. \qquad (32)$$

For $P_{\mathrm{eff}} = -1$ one has a slope of $-(1 - A_{LR})/(1 + A_{LR}) = -0.42$ while one has a much larger positive slope of $(1 + A_{LR})/(1 - A_{LR}) = +2.38$ for $P_{\mathrm{eff}} = +1$. This substantiates the statement made above and in Sec. I about the stability of extrapolations away from $P_{\mathrm{eff}} = \pm 1$. For example, keeping only the linear term in the Taylor expansion of Eq. (31), one has $|\vec{P}| = 0.98$ for $P_{\mathrm{eff}} = -0.95$, while $|\vec{P}|$ drops to $|\vec{P}| = 0.88$ for $P_{\mathrm{eff}} = +0.95$.

For energies above threshold the slope Eq. (32) becomes energy and angle dependent. We do not show plots of the slope at higher energies. We have, however, checked numerically that the above statement about the stability of the $|\vec{P}|$ result at $P_{\mathrm{eff}} = -1$ against variations of P_{eff} remains true at higher energies in the whole angular range, where the slope in the backward region has a tendency to be smaller than in the forward region.

As mentioned above, minimal polarization $|\vec{P}| = 0$ occurs for $P_{\mathrm{eff}} = A_{LR} = 0.409$ for all values of $\cos\theta$. This again shows that an extrapolation away from $P_{\mathrm{eff}} = -1$ is more stable than an extrapolation from $P_{\mathrm{eff}} = +1$ since one is much closer to the polarization zero in the latter case. This observation will carry over to the P_{eff} dependence at higher energies.

In Fig. 7(a) we show the threshold correlation of the angles α and θ for different values of P_{eff}. Starting at $P_{\mathrm{eff}} = -1$ the two angles are related by $\alpha = 180° - \theta$ up to the longitudinal polarization zero at $P_{\mathrm{eff}} = A_{LR} = 0.409$ after which the correlation becomes $\alpha = -\theta$.

As the beam energy increases, the polarization vector of the top quark slowly turns into the direction of its momentum (or opposite to it). Finally, in the high-energy limit $s \to \infty$, when $v \to 1$, the polarization of the top becomes purely longitudinal in the helicity system such that $|\vec{P}| = |P^{(\ell)}|$ since its transverse and normal components involve a spin flip amplitude and thus vanish as $m_t/\sqrt{s}$. Note that, although $P^{(\mathrm{tr})}$ is asymptotically suppressed, it is still sizable at $\sqrt{s} = 1000$ GeV as Fig. 1 shows.

In fact, in the high-energy limit, one has $\vec{P}(\cos\theta) = P^{(\ell)}(\cos\theta) \cdot \hat{p}_t$ with

$$P^{(\ell)}(\cos\theta) = \frac{(g_{14} + g_{41} + P_{\mathrm{eff}}(g_{11} + g_{44}))(1 + \cos\theta)^2 + (g_{14} - g_{41} - P_{\mathrm{eff}}(g_{11} - g_{44}))(1 - \cos\theta)^2}{(g_{11} + g_{44} + P_{\mathrm{eff}}(g_{14} + g_{41}))(1 + \cos\theta)^2 + (g_{11} - g_{44} - P_{\mathrm{eff}}(g_{14} - g_{41}))(1 - \cos\theta)^2} \qquad (33)$$

for the surviving longitudinal polarization. In the same limit, the electroweak coupling coefficients take the numerical values $g_{11} = 0.601$, $g_{14} = -0.131$, $g_{41} = -0.201$, $g_{44} = 0.483$, $g_{12} = 0.352$, and $g_{42} = -0.164$. When $P_{\mathrm{eff}} = -1$ it is more convenient to switch to the chiral electroweak coefficients $f_{LL/LR}$ defined in the Appendix. One has $(f_{LL} = -1.190; f_{LR} = -0.434)$

$$P^{(\ell)}(\cos\theta) = -\frac{1 - b_{LR}}{1 + b_{LR}} \quad \text{with } b_{LR} = \left(\frac{f_{LR}}{f_{LL}}\right)^2 \frac{(1 - \cos\theta)^2}{(1 + \cos\theta)^2}. \qquad (34)$$
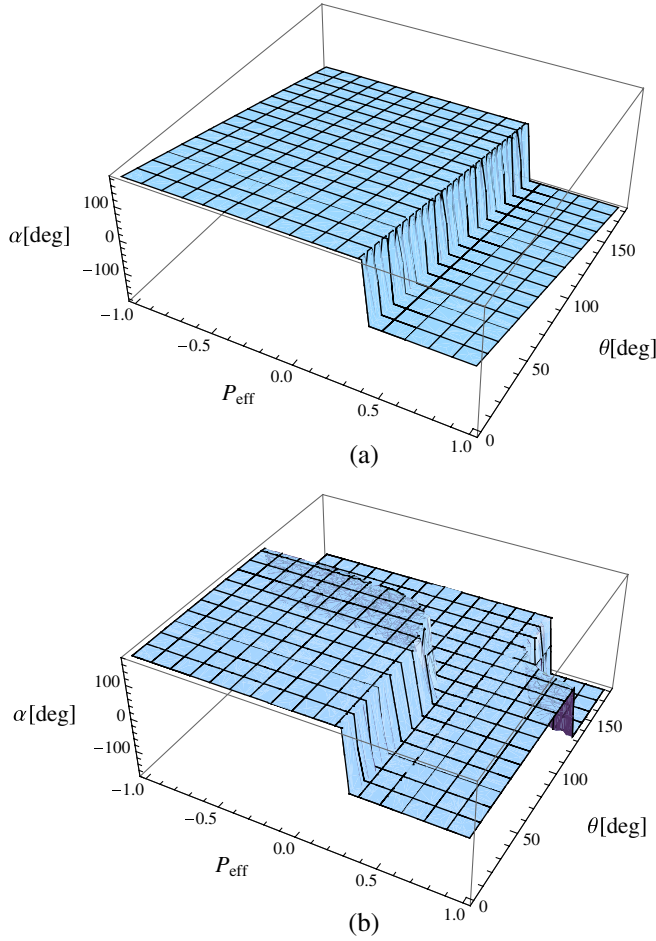
---

[6]As discussed in Sec. II, QCD binding effects significantly modify the naive threshold results in the threshold region.

[7]Threshold simplifications for $(q\bar{q})$ production have also been discussed in Ref. [26]. Similar simplifications for polarization observables occur for the threshold production of gauge boson pairs [27].

FIG. 7 (color online). Correlation of the angles α and θ in dependence on the effective beam polarization P_{eff} (a) for threshold energies $\sqrt{s} = 2m_t$ and (b) for $s \to \infty$.

$P^{(\ell)}$ goes through zero for $b_{LR} = 1$ which is solved by $\cos\theta = -(f_{LL} - f_{LR})/(f_{LL} + f_{LR})$. For $P_{\text{eff}} = +1$ one has a similar simplification where the quantities on the right-hand side of Eq. (34) are replaced by $b_{LR} \to b_{RL}$ and $f_{LL/LR} \to f_{RR/RL}$ ($f_{RR} = -0.867$; $f_{RL} = -0.217$). In this case $P^{(\ell)}$ goes through zero for $b_{RL} = 1$, or for $\cos\theta = -(f_{RR} - f_{RL})/(f_{RR} + f_{RL})$.

At threshold the rate shows no $\cos\theta$ dependence since the $(t\bar{t})$ pair is produced in a S-wave state. This is different in the high-energy limit when $v = 1$, where the forward rate strongly dominates over the backward rate, as an inspection of the denominator of Eq. (33) shows. Since an accurate measurement of the polarization observables requires large statistics, and thus large event samples, the issue of rates is an important one. Numerically, one finds $\sigma(\cos\theta = +1)/\sigma(\cos\theta = -1) = 9.23(1 - 0.31 P_{\text{eff}})/(1 - 0.60 P_{\text{eff}})$. The dependence on P_{eff} is small. When averaging over the forward (F) and backward (B) hemispheres, one finds $\langle\sigma\rangle_F/\langle\sigma\rangle_B = 4.04(1 - 0.31 P_{\text{eff}})/(1 - 0.43 P_{\text{eff}})$, i.e. in the case of unpolarized beams when $P_{\text{eff}} = 0$ the rate in the forward hemisphere dominates over the rate in the

backward hemisphere by a factor of 4 with only slight dependence on beam polarization. Comparing to Eq. (29) the forward dominance is more pronounced in the high-energy limit than at $\sqrt{s} = 500$ GeV.

Equation (33) also very nicely shows how varying P_{eff} affects the longitudinal polarization $P^{(\ell)}$. For the unpolarized beam case $P_{\text{eff}} = 0$ the longitudinal polarization $P^{(\ell)}$ is negative (-31%) at the forward point (FP) $\cos\theta = +1$ and positive ($+60\%$) at the backward point (BP) $\cos\theta = -1$. For maximally polarized beams $P^{\text{eff}} = \pm 1$, Eq. (33) can be seen to satisfy the angular momentum conservation conditions, Eq. (23). For $P^{\text{eff}} = \pm 1$ the longitudinal polarization monotonically increases/decreases from the backward to the forward point. It can be seen to go through zero at $\cos\theta = (g_{11} - g_{41} - g_{12} + g_{42})/(g_{14} - g_{44}) = -0.47(\simeq 117.8°)$ for $P_{\text{eff}} = -1$ and $\cos\theta = -(g_{11} + g_{41} - g_{12} - g_{42})/(g_{14} + g_{44}) = -0.60(\simeq 126.9°)$ for $P_{\text{eff}} = +1$ [see discussion after Eq. (34)]. Close to $P_{\text{eff}} = \pm 1$, the longitudinal polarization zeros are only mildly dependent on P_{eff}. There is a range of P_{eff} values for which the longitudinal polarization remains positive over the whole $\cos\theta$ range. This is determined by the zeros of the coefficients of the angular factors in the numerator of Eq. (33). The condition for positivity of $P^{(\ell)}$ reads

$$-\frac{g_{14} + g_{41}}{g_{11} + g_{44}} < P_{\text{eff}} < \frac{g_{14} - g_{41}}{g_{11} - g_{44}}. \qquad (35)$$

Numerically this translates into $0.31 < P_{\text{eff}} < 0.60$. The same bounding values determine the vanishing of the polarization at the forward and backward points. At the forward point, where the rate is highest, the polarization $|\vec{P}|$ can be made to vanish by setting $P_{\text{eff}} = -(g_{14} + g_{41})/(g_{11} + g_{44}) = 0.31$. At the backward point, one has zero longitudinal polarization for $P_{\text{eff}} = (g_{14} - g_{41})/(g_{11} - g_{44}) = 0.60$.

All of this is illustrated in Fig. 7(b) showing the correlation between P_{eff} and the angles α and θ. The steplike behavior in Fig. 7(b) is associated with the vanishing of the polarization at which points the polarization vector changes its direction by 180°. At $P_{\text{eff}} = -1$ the polarization vector $\vec{P}$ is antiparallel to $\vec{p}_t$ up to where $\vec{P}$ becomes zero at $\theta \sim 117.8°$. From then on $\vec{P}$ is parallel to $\vec{p}_t$. Zero polarization and the location of the steplike behavior is slightly P_{eff} dependent and is shifted to lower values of α. For $0.31 < P_{\text{eff}} < 0.60$ the polarization $\vec{P}$ is always parallel to $\vec{p}_t$. Finally, for $P_{\text{eff}} = +1$ the polarization $\vec{P}$ starts off parallel to $\vec{p}_t$ and turns antiparallel to $\vec{p}_t$ after the zero at $\cos\theta \simeq 126.9°$. Again the polarization zero and the associated steplike behavior is slightly shifted when one moves away from $P_{\text{eff}} = +1$.

Given the fact that the polarization turns from the beam direction to the momentum direction (or its opposite) going from threshold to the high-energy limit it would be interesting to know how fast this transition occurs when the beam energy is ramped up in the envisaged range of beam
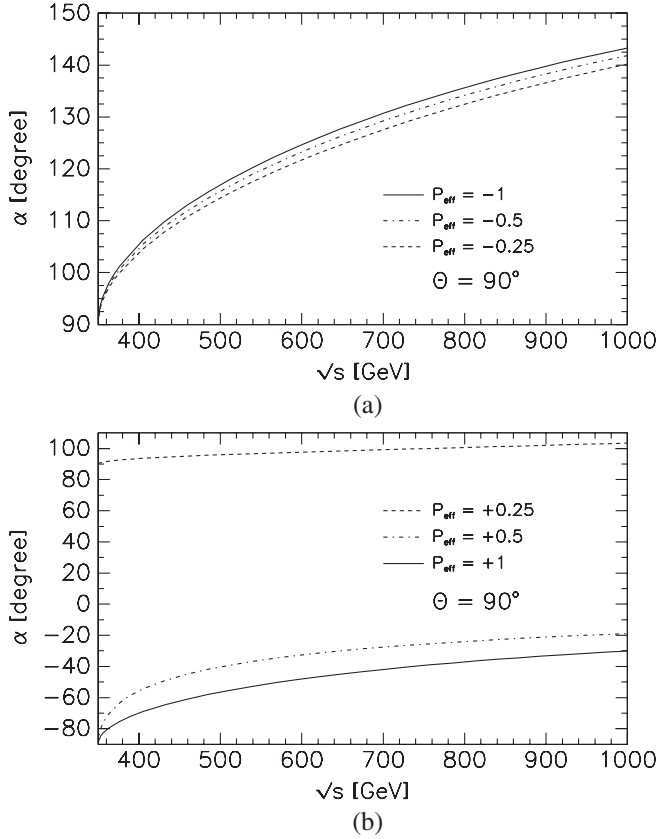
FIG. 8. The top quark polarization angle α for a scattering angle of $\theta = 90°$ as a function of the beam energy for (a) negative values of $P_{\mathrm{eff}} = -1, -0.5, -0.25$ and (b) positive values of $P_{\mathrm{eff}} = +1, +0.5, +0.25$.

energies $\sqrt{s} \sim 2m_t \div 1000$ GeV. In Fig. 8 we investigate the energy dependence of the angle α for several values of P_{eff} for a scattering angle of $\theta = 90°$. In Fig. 8(a) we consider three representative negative values of P_{eff}. All three curves start off with the threshold angle $\alpha = 90°$. The growth of α does not depend much on P_{eff} but is still far away from the asymptotic value $\alpha = 180°$ at $\sqrt{s} = 1000$ GeV. For positive values of P_{eff} the dependence of α on P_{eff} is more pronounced [see Fig. 8(b)]. For $P_{\mathrm{eff}} = +1$ and $P_{\mathrm{eff}} = +0.5$, one is getting closer to the asymptotic value of $\alpha = 0°$ at $\sqrt{s} = 1000$ GeV than for the negative values of P_{eff} shown in Fig. 8(a). The behavior of the $P_{\mathrm{eff}} = +0.25$ curve differs from the two other curves since one has crossed a longitudinal polarization zero between $P_{\mathrm{eff}} = +0.5$ and $P_{\mathrm{eff}} = +0.25$.

V. BORN TERM SIMPLIFICATIONS FOR $P_{\mathrm{eff}} = \mp 1$

As has been emphasized in the notable paper by Parke and Shadmi [5], the Born term polarization formulas considerably simplify for the case of maximal effective beam polarization $P_{\mathrm{eff}} = -1$ which corresponds to a (e_L^-, e_R^+)

configuration. Although designed for the case of top-antitop spin-spin correlations, the results of Ref. [5] are easily adopted to the case of single-spin polarization as also noted in Ref. [6]. From a practical point of view the limiting case $P_{\mathrm{eff}} = -1$ is very interesting since, as was emphasized in Sec. II, one can get quite close to the maximal value $P_{\mathrm{eff}} = -1$ even if the beam polarizations are not close to their maximal values. Similar simplifications occur for the case $P_{\mathrm{eff}} = +1$. In order to distinguish between the two cases we add the suffixes LR and RL for quantities derived for the case $P_{\mathrm{eff}} = -1$ and $P_{\mathrm{eff}} = +1$, respectively.

For the Born term case and in the limit $P_{\mathrm{eff}} = -1$, the polarized numerators (19) and (20) take a factorized form:

$$N_{LR}^{(\ell)}(\cos\theta) = -\tfrac{3}{8}(f_{LL}(\cos\theta + v)$$
$$+ f_{LR}(\cos\theta - v))A_{LR}(\cos\theta)2N_c s, \quad (36)$$

$$N_{LR}^{(\mathrm{tr})}(\cos\theta) = \tfrac{3}{8}\sin\theta\sqrt{1-v^2}(f_{LL} + f_{LR})A_{LR}(\cos\theta)2N_c s, \quad (37)$$

where the common factor $A_{LR}(\cos\theta)$ is given by

$$A_{LR}(\cos\theta) = f_{LL}(1 + v\cos\theta) + f_{LR}(1 - v\cos\theta). \quad (38)$$

We have made use of the chiral electroweak coupling coefficients $f_{LL/LR}$ of Ref. [5] which are simply related to our electroweak coupling factors g_{ij} (see the Appendix). One can check that one can obtain $N_{LR}^{(\ell)}(\cos\theta)$ in Eq. (36) from the generic spin formula Eq. (1) of Ref. [5] when one specifies to the helicity system with $\cos\xi = +1$. Similarly, one obtains $N_{LR}^{(\mathrm{tr})}(\cos\theta)$ in Eq. (37) when one specifies to the transversity system $\cos\xi = 0$. In each of the two respective systems, one has to take the cross section difference $\sigma(t\uparrow) - \sigma(t\downarrow)$.

One can then determine the angle α enclosing the direction of the top quark and its polarization vector by taking the ratio $N^{(\mathrm{tr})}/N^{(\ell)}$. One has

$$\tan\alpha_{LR} = \frac{N_{LR}^{(\mathrm{tr})}(\cos\theta)}{N_{LR}^{(\ell)}(\cos\theta)}$$

$$= -\frac{\sin\theta\sqrt{1-v^2}(f_{LL} + f_{LR})}{f_{LL}(\cos\theta + v) + f_{LR}(\cos\theta - v)}. \quad (39)$$

For example, at threshold ($v = 0$) one has $\tan\alpha_{LR} = -\tan\theta$ with the solution $\alpha_{LR} = 180° - \theta$ in agreement with the corresponding limit in Sec. IV. As another example we take $\theta = 90°$ and obtain $\tan\alpha_{LR} = -(f_{LL} + f_{LR})/(f_{LL} - f_{LR}) \cdot \sqrt{1-v^2}/v$. For $\sqrt{s} = 500$ GeV this gives $\alpha_{LR} = 124.9°$, i.e. the polarization vector is still close to its threshold value of $\alpha_{LR} = 90°$ but has started to turn to its asymptotic value of $\alpha_{LR} = 180°$.

Equation (39) is nothing but the defining equation for the off-diagonal basis in Ref. [5] considering the fact that their

angle ξ is related to α_{LR} by $\xi = 180° - \alpha_{LR}$. In the coordinate system where the z axis is defined by the angle α_{LR} given in Eq. (39), the polarization vector of the top quark is purely longitudinal. In particular, this means that its transverse component is zero in the off-diagonal basis implying that the density matrix of the top quark is diagonal in this basis. In this sense the "off-diagonal" basis is a diagonal basis and the wording "off-diagonal" used in Ref. [5] for this basis can lead to a misunderstanding.

A different but equivalent view on the off-diagonal basis may be obtained by rotating the nondiagonal helicity system density matrix of the top quark ($m, n = \pm 1/2$)

$$\rho_{mn} = \frac{1}{2}\begin{pmatrix} 1 + P^{(\ell)} & P^{(\mathrm{tr})} \\ P^{(\mathrm{tr})} & 1 - P^{(\ell)} \end{pmatrix} = \frac{1}{2}(\sigma \cdot \mathbb{1} + \vec{\xi} \cdot \vec{\sigma}) \tag{40}$$

in the scattering plane by an angle α. One has

$$\rho'_{m'n'} = d^{1/2}_{m'm}(\alpha)\rho_{mn}d^{1/2\dagger}_{nn'}(\alpha) = \frac{1}{2}\begin{pmatrix} 1 + (P^{(\ell)}\cos\alpha + P^{(\mathrm{tr})}\sin\alpha) & P^{(\ell)}\sin\alpha - P^{(\mathrm{tr})}\cos\alpha \\ P^{(\ell)}\sin\alpha - P^{(\mathrm{tr})}\cos\alpha & 1 - (P^{(\ell)}\cos\alpha + P^{(\mathrm{tr})}\sin\alpha) \end{pmatrix}$$

$$\rightarrow \frac{1}{2}\begin{pmatrix} 1 + |\vec{P}| & 0 \\ 0 & 1 - |\vec{P}| \end{pmatrix}, \tag{41}$$

where $d^{1/2}_{m'm}(\alpha)$ is the usual spin-1/2 Wigner rotation matrix and $|\vec{P}| = \sqrt{P^{(\ell)2} + P^{(\mathrm{tr})2}}$. It is evident that a rotation by the angle $\alpha = \alpha_{LR}$ defined in Eq. (39) diagonalizes the original density matrix as indicated in the last line of Eq. (41).

The correlation between the angles α (for general values of P_{eff}) and θ are shown in the contour plots Fig. 9. In Fig. 9(a) we choose $P_{\mathrm{eff}} = -1$ and show fixed energy contours in the (α, θ) plane for several values of the c.m. energy $\sqrt{s}$. Up to $\sqrt{s} = 1000$ GeV the correlations do not deviate very much from the threshold correlation $\alpha = 180° - \theta$. In the limit $v = 1$, one has a steplike behavior of the correlation function as discussed before in Sec. IV. In Fig. 9(b) we show the same plots for $P_{\mathrm{eff}} = +1$. The approach of the correlation curves to the steplike behavior at $v = 1$ is somewhat faster than in the case $P_{\mathrm{eff}} = -1$. In Fig. 9(c) we show the same curves for $P_{\mathrm{eff}} = 0.5$ where one is close to the polarization zero. The $\sqrt{s} = 360$ GeV correlation curve is still close to the corresponding threshold curve $\alpha = -\theta$. At higher energies one sees a different behavior in as much as the correlation curves run into $\alpha = 0°$ at the backward point as does the flat asymptotic curve as discussed before in Sec. 4 (Fig. 7).

In order to calculate the normalized polarization components, one needs also the denominator factor $D(\cos\theta)$ in Eq. (22), again for the Born term case and $P_{\mathrm{eff}} = -1$. One has

$$D_{LR}(\cos\theta) = \tfrac{3}{8}(A^2_{LR} - 2f_{LL}f_{LR}v^2\sin^2\theta)2N_c s \tag{42}$$

proportional to the cross section sum $\sigma(t\uparrow) + \sigma(t\downarrow)$ in any of the systems in Ref. [5].

Using Eqs. (36) and (42) the longitudinal polarization $P^{(\ell)}_{LR} = N^{(\ell)}_{LR}/D_{LR}$ can be seen to become maximally -1 and $+1$ in the forward and backward directions, respectively, in agreement with angular momentum conservation as before. One also reproduces the threshold

formula Eq. (30) and the high-energy formula Eq. (33) when these are specified to $P_{\mathrm{eff}} = -1$. The longitudinal polarization goes through zero at

$$\cos\theta_0 = -\frac{f_{LL} - f_{LR}}{f_{LL} + f_{LR}}v$$
$$= \frac{g_{14} - g_{44}}{g_{11} - g_{41} + g_{12} - g_{42}}v \qquad (= -0.48v). \tag{43}$$

At this value of $\cos\theta$ the polarization vector of the top quark is orthogonal to its momentum. Later on we shall see that, at this point, $P^{(\mathrm{tr})}$ acquires its maximal value and $|\vec{P}|$ acquires its minimal value. Since the ratio $(f_{LL} - f_{LR})/(f_{LL} + f_{LR})$ is only mildly energy dependent, the location of the zero is mainly determined by the velocity of the top quark, i.e. it moves towards the backward point when the energy is increased. For convenience we have added the $\sqrt{s} = 500$ GeV value of the electroweak coupling ratio in brackets in Eq. (43).

The transverse polarization $P^{(\mathrm{tr})}_{LR}$ vanishes in the forward and backward directions due to angular momentum conservation, as is explicit in Eq. (37). It becomes maximal at the point where the longitudinal polarization goes through zero. This can be verified by an explicit calculation, viz.

$$\frac{dP^{(\mathrm{tr})}_{LR}}{d\cos\theta}\bigg|_{\cos\theta_0} = 0, \tag{44}$$

where $\cos\theta_0$ is given in Eq. (43).

Whereas there are no illuminating expressions for the longitudinal and transverse polarization components for general values of the velocity v, the magnitude of the polarization $|\vec{P}|$ for $P_{\mathrm{eff}} = -1$ takes the simple form

$$|\vec{P}_{LR}| = \frac{\sqrt{N^{(\ell)2}_{LR} + N^{(\mathrm{tr})2}_{LR}}}{D_{LR}} = \frac{\sqrt{1 - 4a_{LR}}}{1 - 2a_{LR}}$$
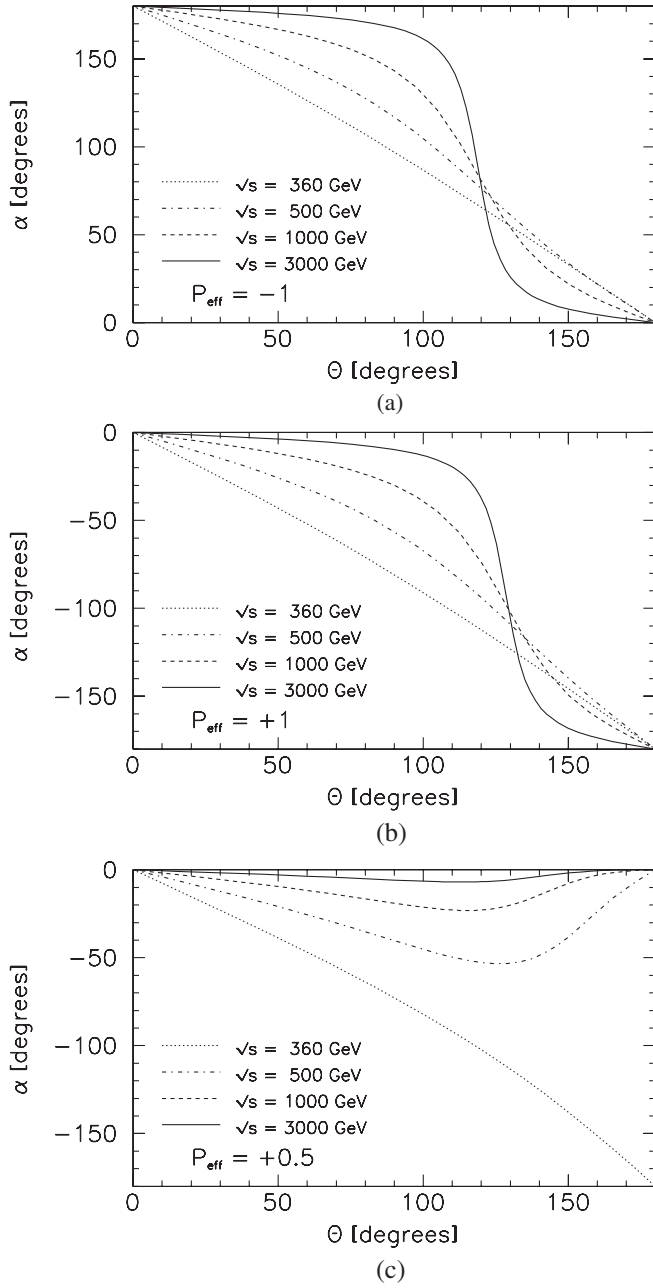$$= 1 - 2a^2_{LR} - 8a^3_{LR} - 18a^3_{LR}\ldots, \tag{45}$$

FIG. 9.   Correlation of angles α and θ for (a) $P_{\text{eff}} = -1$ ($\alpha = \alpha_{LR}$), (b) $P_{\text{eff}} = +1$ ($\alpha = \alpha_{RL}$), and (c) $P_{\text{eff}} = +0.5$ for different values of the c.m. energy $\sqrt{s} = 360$, 500, 1000, and 3000 GeV (notation as in Fig. 5).

where the coefficient a_{LR} depends on $\cos\theta$ through

$$a_{LR}(\cos\theta) = \frac{f_{LL}f_{LR}}{A_{LR}^2(\cos\theta)} v^2 \sin^2\theta. \qquad (46)$$

The convergence of the expansion in Eq. (45) is rather slow except for very small values of a_{LR}. Note that the expansion in Eq. (45) deviates from 1 only at $O(a_{LR}^2)$. At the forward and backward points where $a_{LR} = 0$, one has $|\vec{P}_{LR}| = 1$ as stated before. Between the forward and

backward points the polarization remains reasonably large. For example, for $\sqrt{s} = 500$ GeV the polarization never drops below $|\vec{P}_{LR}| = 0.95$. Differentiating of Eq. (45) with respect to $\cos\theta$, one can see that the minimum of $|\vec{P}_{LR}|$ occurs at the point where the longitudinal polarization $P_{LR}^{(\ell)}$ vanishes [see Eq. (43)], i.e. where the polarization is purely transverse. The high-energy limit of Eq. (45) is discussed in Sec. IV.

Similar simplifications occur for the case $P_{\text{eff}} = +1$ which corresponds to the (e_R^-, e_L^+) configuration. This is effected by the replacement $f_{LL} \rightarrow f_{RR}$ and $f_{LR} \rightarrow f_{RL}$ with a corresponding change in the notation A_{LR}, $a_{LR} \rightarrow A_{RL}$, a_{RL}. Further, one has $N_{RL}^{(\ell)} = -N_{LR}^{(\ell)}(f_{LL} \rightarrow f_{RR}; f_{LR} \rightarrow f_{RL})$ and $N_{RR}^{(\text{tr})} = -N_{LL}^{(\text{tr})}(f_{LL} \rightarrow f_{RR}; f_{LR} \rightarrow f_{RL})$. The zero of $P^{(\ell)}$ is now located at $\cos\theta_0 = -0.63v$ for $\sqrt{s} = 500$ GeV, i.e. the zero is closer to the backward point than in the case $P_{\text{eff}} = -1$. For $\theta = 90°$ the angle α_{RL} can be calculated from $\tan\alpha_{RL} = -(f_{RR} + f_{RL})/(f_{RR} - f_{RL}) \cdot \sqrt{1 - v^2}/v$ which, at $\sqrt{s} = 500$ GeV, gives $\alpha_{RL} = -48°$. At $\cos\theta = 0$ and $\sqrt{s} = 500$ GeV, one has $a_{LR} > a_{RL}$ leading to $|\vec{P}_{LR}| < |\vec{P}_{RL}|$, i.e. the (e_R^-, e_L^+) configuration leads to larger values of the polarization than the (e_L^-, e_R^+) configuration at this point of parameter space. In Fig. 9(b) we show a contour plot in the (α_{RL}, θ) plane for several values of the c.m. energy $\sqrt{s}$. As is the case for the (α_{LR}, θ) correlations, the (α_{RL}, θ) correlations do not deviate very much from the threshold correlation $\alpha = -\theta$ up to $\sqrt{s} = 1000$ GeV.

As a last point we discuss how the polarization angle α_{LR} changes when going from LO to NLO. In Fig. 10 we show a plot of the $\cos\theta$ dependence of the difference $\Delta\alpha_{LR} = \alpha_{LR}(\text{NLO}) - \alpha_{LR}(\text{LO})$ for different energies. The maximal values of the difference occur at values of $\cos\theta$ where the polarization vector is perpendicular to the top quark's momentum, i.e. where $\alpha_{LR} = 90°$ [see discussion after Eq. (43)]. The difference can become as big as $10°$ for $\sqrt{s} = 3000$ GeV. The radiative corrections can
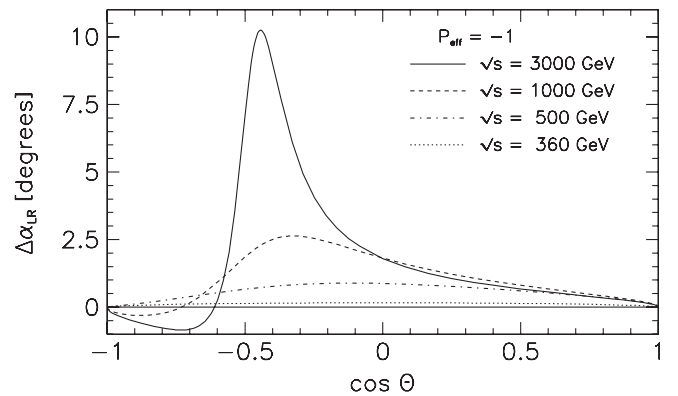

FIG. 10.   Difference $\Delta\alpha_{LR} = \alpha_{LR}(\text{NLO}) - \alpha_{LR}(\text{LO})$ of NLO and LO polarization angles for $\sqrt{s} = 360$, 500, 1000, and 3000 GeV (notation as in Fig. 5).

thus be seen to rotate the polarization vector away from the off-diagonal basis by a nonnegligible amount.

VI. THE POLARIZATION COMPONENTS $P^{(\ell)}$, $P^{(\mathrm{tr})}$, AND $P^{(n)}$

We now turn to the numerical discussion of the three polarization components $P^{(\ell)}$, $P^{(\mathrm{tr})}$, and $P^{(n)}$ keeping in mind the Born term simplifications for $P^{(\ell)}$ and $P^{(\mathrm{tr})}$ discussed in Secs. IV and V. We start our discussion with the longitudinal component $P^{(\ell)}$. In Fig. 11(a) we show the dependence of the NLO longitudinal polarization $P^{(\ell)}$ on $\cos\theta$ at $\sqrt{s} = 500$ GeV for several values of P_{eff} spanning the whole parameter range of P_{eff}. The dependence of $P^{(\ell)}$ on P_{eff} and $\cos\theta$ is quite pronounced. For $P_{\mathrm{eff}} = \pm 1$ the $\cos\theta$ dependence already deviates considerably from the (Born term) threshold behavior $P^{(\ell)} = \pm\cos\theta$. It is quite interesting to observe that all NLO curves intersect at one point where $\cos\theta = -0.406$. This can be verified by setting to zero the derivative of $P^{(\ell)}$ with respect to P_{eff}. The relevant higher order equation admits of a solution at the above value of $\cos\theta$. In Fig. 11(b) we show the $\cos\theta$ dependence of $P^{(\ell)}$ for several energies keeping P_{eff} fixed at $P_{\mathrm{eff}} = -1$. At the resolution of the figure all curves seemingly go through -1 and $+1$ at the forward and backward point, respectively, showing that hard gluon emission effects are not very strong at these energies. The energy dependence is not very pronounced, even if the $\sqrt{s} = 500$ GeV curve already deviates from the threshold behavior $P^{(\ell)} = -\cos\theta$.

The strong dependence of $P^{(\ell)}$ on P_{eff} can be nicely exposed by considering the LO expression for the polar mean $\langle P^{(\ell)}\rangle$ which is obtained by integrating the numerator and the denominator in Eq. (18) separately over $\cos\theta$. One obtains
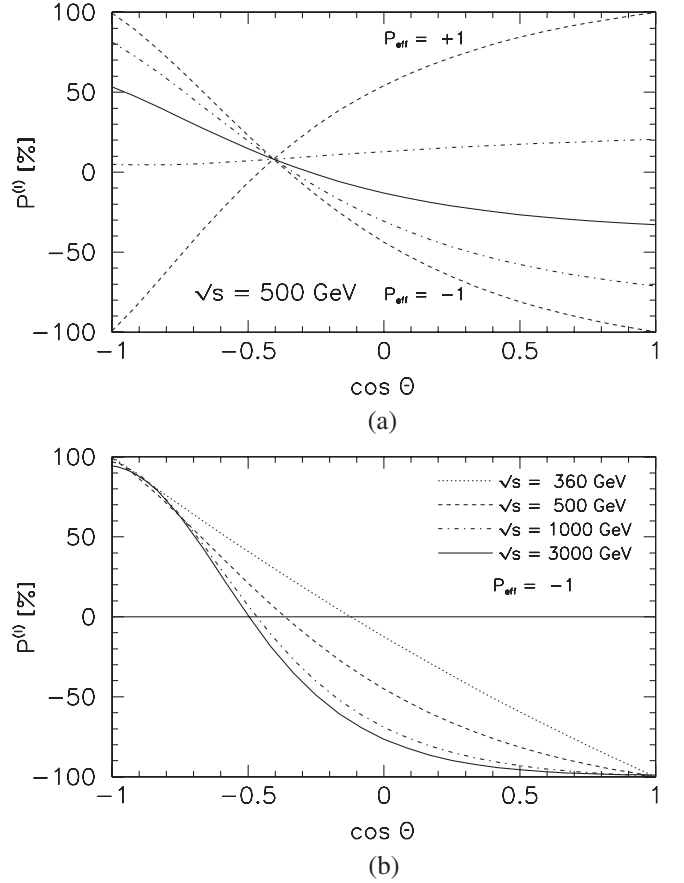

(a)

(b)

FIG. 11.   NLO longitudinal top polarization as a function of $\cos\theta$ drawn (a) for effective beam polarizations $P_{\mathrm{eff}} = -1, -0.5, 0, +0.5, +1$ (notation as in Fig. 1) at $\sqrt{s} = 500$ GeV; (b) at beam energies $\sqrt{s} = 360, 500, 1000,$ and 3000 GeV (notation as in Fig. 5) and $P_{\mathrm{eff}} = -1$.

$$\langle P^{(\ell)}\rangle = \frac{\langle N^{(\ell)}\rangle}{\langle D\rangle} = \frac{4}{3}v\frac{g_{14} + g_{44}P_{\mathrm{eff}}}{(g_{11} + g_{41}P_{\mathrm{eff}})(1 + v^2/3) + (g_{12} + g_{42}P_{\mathrm{eff}})(1 - v^2)}. \tag{47}$$

$\langle P^{(\ell)}\rangle$ vanishes at threshold. In the high-energy limit, one has $\langle P^{(\ell)}\rangle = (g_{14} + g_{44}P_{\mathrm{eff}})/(g_{11} + g_{41}P_{\mathrm{eff}})$ which, for $P_{\mathrm{eff}} = \pm 1$, gives $\langle P^{(\ell)}\rangle = 0.882$ and $\langle P^{(\ell)}\rangle = -0.766$ close to the $\sqrt{s} = 1000$ GeV values in Fig. 1. At $\sqrt{s} = 500$ GeV, one has

$$\langle P^{(\ell)}\rangle = \langle P^{(\ell)}\rangle(P_{\mathrm{eff}} = 0)\frac{1 - 3.61P_{\mathrm{eff}}}{1 - 0.37P_{\mathrm{eff}}}$$
$$= \begin{cases} +0.62 & P_{\mathrm{eff}} = +1 \\ -0.15 & = 0 \\ -0.50 & = -1 \end{cases}. \tag{48}$$

One observes a strong dependence of the mean longitudinal polarization on P_{eff}. By comparing with the

$\sqrt{s} = 500$ GeV point in Fig. 1(a), one observes a 2% change in $\langle P^{(\ell)}\rangle$ due to the radiative corrections.

The same strong dependence on P_{eff} is found when one averages over the forward hemisphere where one has ($\sqrt{s} = 500$ GeV)

$$\langle P^{(\ell)}\rangle_F = \langle P^{(\ell)}\rangle_F(P_{\mathrm{eff}} = 0)\frac{1 - 3.09P_{\mathrm{eff}}}{1 - 0.34P_{\mathrm{eff}}}$$
$$= \begin{cases} +0.85 & P_{\mathrm{eff}} = +1 \\ -0.27 & = 0 \\ -0.81 & = -1 \end{cases}. \tag{49}$$

When one averages over the backward hemisphere the average longitudinal polarization is smaller and the dependence on P_{eff} is much weaker viz.

$$\langle P^{(\ell)}\rangle_B = \langle P^{(\ell)}\rangle_B(P_{\rm eff}=0)\frac{1-1.04P_{\rm eff}}{1-0.43P_{\rm eff}}$$

$$= \begin{cases} -0.01 & P_{\rm eff}=+1 \\ +0.13 & =0 \\ +0.18 & =-1 \end{cases}. \tag{50}$$

In Fig. 12(a) we show a plot of the energy dependence of the forward and backward averages of the longitudinal polarizations for $P_{\rm eff}=-1$. The forward average $\langle P^{(\ell)}\rangle_F$ is large and negative. It starts with a nominal threshold value of $\langle P^{(\ell)}\rangle_F=-0.5$ and slowly drops to a value of $\langle P^{(\ell)}\rangle_F=-0.90$ at $\sqrt{s}=1000$ GeV which is not far from the asymptotic Born term value $\langle P^{(\ell)}\rangle_F=-(7f_{LL}^2-f_{LR}^2)/(7f_{LL}^2+f_{LR}^2)=-0.96$. The backward average $\langle P^{(\ell)}\rangle_B$ is smaller and positive. It drops from a nominal threshold value of $\langle P^{(\ell)}\rangle_B=+0.5$ to $\langle P^{(\ell)}\rangle_B=+0.14$ at $\sqrt{s}=1000$ GeV as compared to the asymptotic Born term value $\langle P^{(\ell)}\rangle_B=-(f_{LL}^2-7f_{LR}^2)/(f_{LL}^2+7f_{LR}^2)=-0.04$.

We now turn to the transverse polarization component $P^{(\rm tr)}$. Similar to Figs. 11(a) and 11(b) we show the corre-
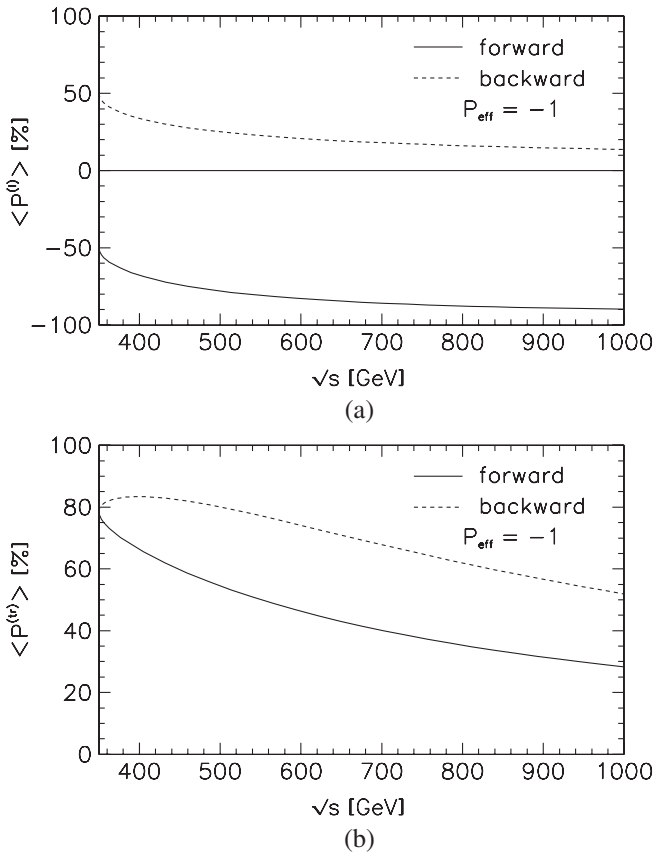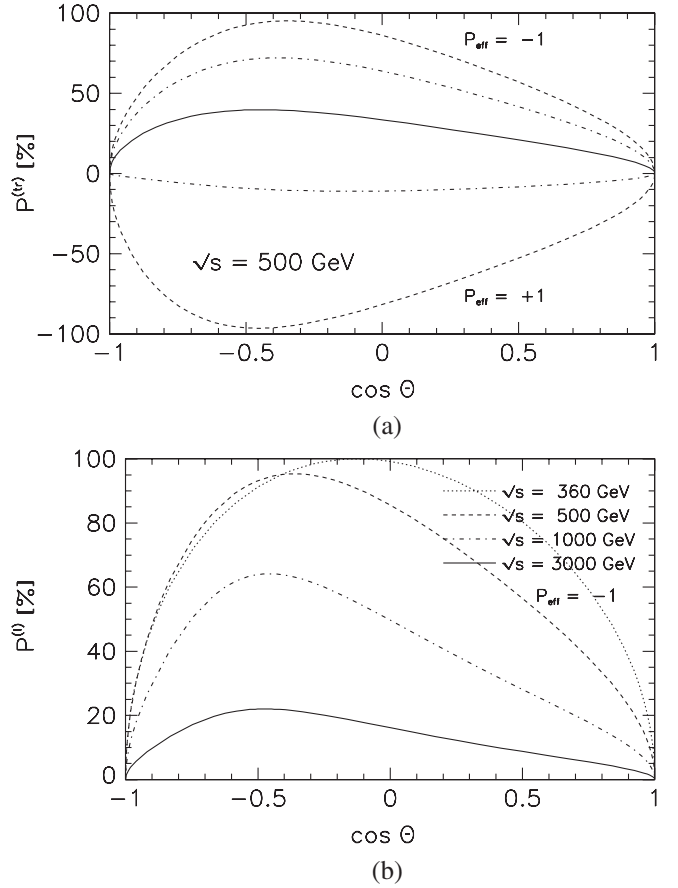

(a)

(b)

FIG. 13. NLO transverse top polarization as a function of the scattering angle θ drawn (a) for effective beam polarizations $P_{\rm eff}=-1,-0.5,0,+0.5,+1$ (notation as in Fig. 1) at $\sqrt{s}=500$ GeV; (b) at beam energies $\sqrt{s}=360,500,1000,$ and 3000 GeV (notation as in Fig. 5) and $P_{\rm eff}=-1$.

(a)

(b)

FIG. 12. Average (a) longitudinal polarization $\langle P^{(l)}\rangle$ and (b) transverse polarization $\langle P^{(\rm tr)}\rangle$ in the forward and backward hemispheres for $P_{\rm eff}=-1$.

sponding curves for $P^{(\rm tr)}$ in Figs. 13(a) and 13(b). The transverse polarization vanishes at the end points due to the overall $\sin\theta$ factor in the angular decay distribution [Eq. (20)]. The dependence on $P_{\rm eff}$ is again quite pronounced. One observes a faster change with $P_{\rm eff}$ at $P_{\rm eff}=+1$ than at $P_{\rm eff}=-1$. $P^{(\rm tr)}$ vanishes close to $P_{\rm eff}=+0.5$. At $\sqrt{s}=500$ GeV the deviations from the threshold behavior $P^{(\rm tr)}=\pm\sqrt{1-\cos\theta^2}$ for $P_{\rm eff}=\pm1$ are slight but clearly visible. The $(\sqrt{s})^{-1}$ dependence of the transverse polarization is easily discernible in Fig. 13(b). A visual inspection shows that, as is exact in the Born term case for $P_{\rm eff}=\pm1$, the NLO longitudinal and transverse polarization components are complementary in the sense that the transverse polarization becomes maximal very close to the point where the longitudinal polarization becomes minimal, and vice versa. This observation bodes well for the existence of large values of the total polarization as discussed in Sec. VII.

For the mean value of the transverse polarization, one obtains the Born term level expression

$$\langle P^{(\mathrm{tr})}\rangle = -\frac{\pi}{2}\frac{m_t}{\sqrt{s}}\frac{g_{41} + g_{42} + (g_{11} + g_{12})P_{\mathrm{eff}}}{(g_{11} + g_{41}P_{\mathrm{eff}})(1 + v^2/3) + (g_{12} + g_{42}P_{\mathrm{eff}})(1 - v^2)}. \qquad (51)$$

At nominal threshold one has $\langle P^{(\mathrm{tr})}\rangle = \mp\pi/4$ for $P_{\mathrm{eff}} = \pm1$ close to what is seen in Fig. 1. In the high-energy limit $\langle P^{(\mathrm{tr})}\rangle$ vanishes as $(\sqrt{s})^{-1}$. At $\sqrt{s} = 500$ GeV one has

$$\langle P^{(\mathrm{tr})}\rangle = \langle P^{(\mathrm{tr})}\rangle(P_{\mathrm{eff}} = 0)\frac{1 - 2.53P_{\mathrm{eff}}}{1 - 0.37P_{\mathrm{eff}}}$$

$$= \begin{cases} -0.57 & P_{\mathrm{eff}} = +1 \\ +0.24 & = 0 \\ +0.61 & = -1 \end{cases}, \qquad (52)$$

showing again the large effect of beam polarization. By comparing with the $\sqrt{s} = 500$ GeV point in Fig. 1(b), one observes a 1.5% change in $\langle P^{(\mathrm{tr})}\rangle$ due to the radiative corrections.

For the ratio of the forward and backward mean of the transverse polarization, one obtains

$$\frac{\langle P^{(\mathrm{tr})}\rangle_F}{\langle P^{(\mathrm{tr})}\rangle_B} = \frac{\langle N^{(\mathrm{tr})}\rangle_F}{\langle N^{(\mathrm{tr})}\rangle_B}\frac{\langle\sigma\rangle_B}{\langle\sigma\rangle_F} = \begin{cases} +0.54 & P_{\mathrm{eff}} = +1 \\ +0.53 & = 0 \\ +0.61 & = -1 \end{cases}. \qquad (53)$$

There is a slight dominance of the backward mean as also evident in Fig. 13. The dependence of the ratio (53) on P_{eff} is not very pronounced.

A plot of the energy dependence of the forward and backward averages of the transverse polarization is shown in Fig. 12(b). Both curves start at the nominal threshold value $\langle P^{(\mathrm{tr})}\rangle_F = \langle P^{(\mathrm{tr})}\rangle_B = \pi/4$ and then quite slowly begin their descent to their asymptotic demise. At $\sqrt{s} = 500$ GeV and $P_{\mathrm{eff}} = -1$, one can compare the NLO result for $\langle P^{(\mathrm{tr})}\rangle_F/\langle P^{(\mathrm{tr})}\rangle_B = 0.68$ with the corresponding LO result $\langle P^{(\mathrm{tr})}\rangle_F/\langle P^{(\mathrm{tr})}\rangle_B = 0.61$ in Eq. (53).

The normal polarization component $P^{(n)}$ is a T-odd observable and thus obtains only contributions from the imaginary parts of the production amplitudes. Since we are neglecting the contribution from the imaginary part of the Z propagator, the only contribution to the normal polarization component $P^{(n)}$ at $O(\alpha_s)$ is that of the imaginary part of the one-loop contributions [Eqs. (14) and (15)]. When averaging over $\cos\theta$, the contributions of $H_I^{1,2(n)}$(loop) drop out and one has the $O(\alpha_s)$ result

$$\langle P^{(n)}\rangle = -\alpha_s\frac{\pi}{6}\frac{m_t}{\sqrt{s}}(2 - v^2)\frac{g_{44} + g_{14}P_{\mathrm{eff}}}{(g_{11} + g_{41}P_{\mathrm{eff}})(1 + v^2/3) + (g_{12} + g_{42}P_{\mathrm{eff}})(1 - v^2)}. \qquad (54)$$

Numerically one has ($\sqrt{s} = 500$ GeV; $\alpha_s = 0.094$)

$$\langle P^{(n)}\rangle = \langle P^{(n)}\rangle(P_{\mathrm{eff}} = 0)\frac{1 - 0.27P_{\mathrm{eff}}}{1 - 0.37P_{\mathrm{eff}}}$$

$$= \begin{cases} -0.015 & P_{\mathrm{eff}} = +1 \\ -0.013 & = 0 \\ -0.012 & = -1 \end{cases}. \qquad (55)$$

Clearly the normal polarization component is small being an $O(\alpha_s)$ effect. Also, the dependence of $\langle P^{(n)}\rangle$ on the beam polarization is quite small.

In Fig. 14 we show the $\cos\theta$ dependence of the normal component of the polarization of the top quark. In Fig. 14 (a) we keep the energy fixed at $\sqrt{s} = 500$ GeV and vary P_{eff}. The differential distribution peaks at around $\cos\theta = 0$ where the peak moves to the left with increasing values of P_{eff}. The peak values of $P^{(n)}$ are around -2%. The dependence on P_{eff} is weak as also evident in Eq. (55). In Fig. 14 (b) we plot the $\cos\theta$ dependence for different energies keeping P_{eff} fixed at $P_{\mathrm{eff}} = -1$. As expected, the normal polarization can be seen to decrease with the typical $(\sqrt{s})^{-1}$ behavior. We mention that we are now in agreement with

the results of Ref. [4] when one takes account of the fact that their normal direction is defined opposite to ours.

Let us close this section by comparing our results to those of the authors of Ref. [6] who calculated $O(\alpha_s)$ radiative corrections to rates into definite spin states in generic coordinate systems starting from the initial beam configurations (e_L^-, e_R^+) and (e_R^-, e_L^+) which correspond to $P_{\mathrm{eff}} = -1$ and $P_{\mathrm{eff}} = +1$, respectively. Put in a different language, they compute radiative corrections to the (unnormalized) diagonal spin density matrix elements $\sigma_\uparrow$ and $\sigma_\downarrow$. In the helicity system, where they use the notation $\sigma_{\downarrow/\uparrow} \equiv \sigma_{L/R}$, their polarized rates $\sigma_{L/R}$ are related to our longitudinal polarization component $P^{(\ell)}$ via

$$\sigma_{L/R} = \frac{\sigma}{2}(1 \mp P^{(\ell)}). \qquad (56)$$

Comparing to the (e_L^-, e_R^+) subdominant spin rate ratio at $\sqrt{s} = 400$ GeV in Table 3 of Ref. [6], we find a -1.34% reduction relative to the LO rate ratio vs their reduction of -1.19%. We consider the two results to be consistent with each other within rounding errors. We mention that our NLO results have been checked before in Ref. [4].
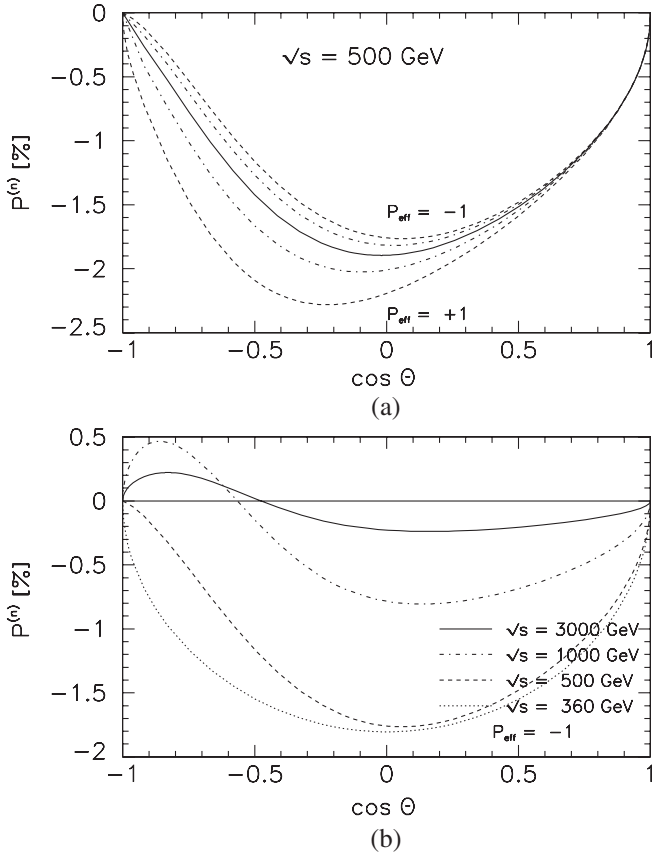
FIG. 14. $O(\alpha_s)$ normal polarization $P^{(n)}$ of the top quark as a function of $\cos\theta$ (a) for effective beam polarizations $P_{\text{eff}} = -1, -0.5, 0, +0.5, +1$ (notation as in Fig. 1) at $\sqrt{s} = 500$ GeV; (b) for $P_{\text{eff}} = -1$ at beam energies $\sqrt{s} = 360, 500, 1000$, and $\sqrt{s} = 3000$ GeV (notation as in Fig. 5).

VII. TOTAL POLARIZATION AND ORIENTATION OF THE POLARIZATION VECTOR

The magnitude of the polarization (also called total polarization) is given by

$$|\vec{P}| = \sqrt{(P^{(\ell)})^2 + (P^{(\text{tr})})^2 + (P^{(n)})^2}. \qquad (57)$$

In Fig. 15 we show the NLO dependence of $|\vec{P}|$ on $\cos\theta$ at different values of $\sqrt{s}$ for the three different values of $P_{\text{eff}} = \pm1$ and 0. As a general feature, one observes that the magnitude of the polarization decreases with energy. When $P_{\text{eff}} = \pm1$, one obtains large values of $|\vec{P}|$, in particular in the forward hemisphere. For example, for $\sqrt{s} = 500$ GeV $|\vec{P}|$ remains above 95% over the whole angular range for $P_{\text{eff}} = \pm1$. The polarization is slightly larger for $P_{\text{eff}} = +1$ than for $P_{\text{eff}} = -1$. At $\sqrt{s} = 360$ GeV and $P_{\text{eff}} = \pm1$, one is still very close to the flat threshold behavior $|\vec{P}| = 1$, whereas for $P_{\text{eff}} = 0$ one observes a slight falloff behavior going from the backward to the forward point. Even for the largest energy
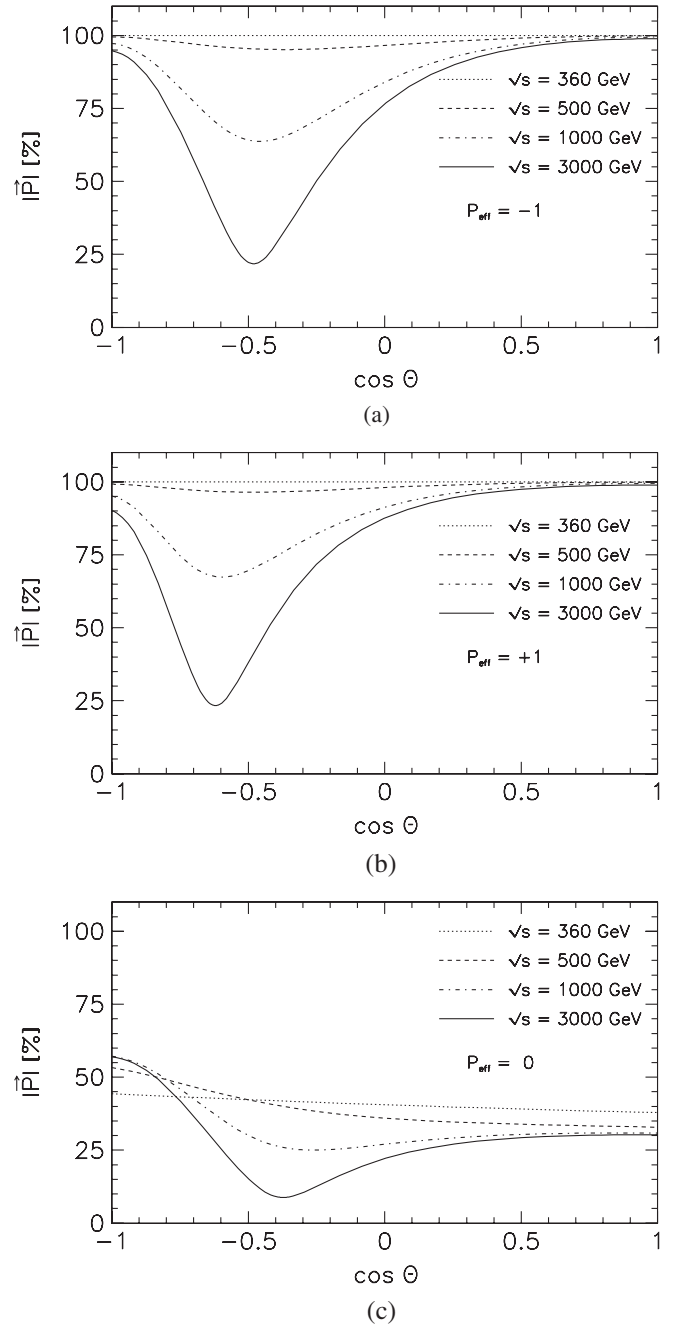

FIG. 15.   Total NLO top quark polarization as a function of $\cos\theta$ for beam energies $\sqrt{s} = 360, 500, 1000$, and 3000 GeV (notation as in Fig. 5) and (a) $P_{\text{eff}} = -1$, (b) $P_{\text{eff}} = +1$, and (c) $P_{\text{eff}} = 0$.

$\sqrt{s} = 3000$ GeV, one does not have a zero for $|\vec{P}|$ showing that one is still away from the asymptotic $v = 1$ case since asymptotically one has polarization zeros for the three cases $P_{\text{eff}} = \pm1, 0$ as discussed in Sec. IV and exhibited in Fig. 7. As mentioned before there is also a very small $O(\alpha_s)$ normal component of the polarization vector which will contribute to $|\vec{P}|$ at the $O(0.01)$. It is so small that it is not discernible in our numerical plots.

In Fig. 16 we show a plot of the energy dependence of the polar average $\langle|\vec{P}|\rangle$ of the total polarization. For both $P_{\text{eff}} = \pm 1$ the average polarization is large in the whole energy range with a slight decrease when the energy is increased. The $P_{\text{eff}} = +1$ polarization is slightly larger than the $P_{\text{eff}} = -1$ polarization. The average total polarization becomes smaller when the effective polarization is reduced from $P_{\text{eff}} = \pm 1$. As has been discussed before the rate of decrease is much faster for $P_{\text{eff}} = +1$ than for $P_{\text{eff}} = -1$ as can be appreciated by comparing the $P_{\text{eff}} = -0.5$ and $P_{\text{eff}} = +0.5$ curves. The smallest polarization in Fig. 16 is obtained for $P_{\text{eff}} = +0.5$. As will be discussed further on $P_{\text{eff}} = +0.5$ is close to the effective beam polarization where one has minimal polarization.

Of interest is the total polarization in the forward and backward hemispheres. In Fig. 17 we show plots of the average total polarization $\langle|\vec{P}|\rangle_{F/B}$ for $P_{\text{eff}} = \pm 1, 0$, where the averaging is done over the forward and backward hemispheres. The average total polarization $\langle|\vec{P}|\rangle_F$ in the forward hemisphere is quite large for both $P_{\text{eff}} = \pm 1$ and remains larger than 95% even up to $\sqrt{s} = 1000$ GeV. This is quite welcome from the point of view of statistics since the bulk of the rate is in the forward hemisphere. The $P_{\text{eff}} = +1$ polarization is slightly larger than the $P_{\text{eff}} = -1$ polarization. The average backward polarization $\langle|\vec{P}|\rangle_B$ is significantly smaller than the forward polarization $\langle|\vec{P}|\rangle_F$ for both $P_{\text{eff}} = \pm 1$ as can also be appreciated by looking at Fig. 15. Both forward and backward $P_{\text{eff}} = 0$ polarizations show a slightly decreasing energy behavior starting at the common threshold value of $\langle|\vec{P}|\rangle = A_{RL} = 0.409$.

Returning to Fig. 15(b) ($P_{\text{eff}} = +1$), one observes a conspicuously large 10% radiative correction at the backward point for $\sqrt{s} = 3000$ GeV where the Born term prediction is $|\vec{P}| = 1$. One can attempt to understand this large value by substituting the asymptotic values of the radiative corrections calculated in Ref. [28]. For the surviving longitudinal component $P^{(\ell)}$, one obtains

FIG. 16. Average NLO top quark polarization $\langle|\vec{P}|\rangle$ for a scattering angle of $\theta = 90°$ as a function of the beam energy $\sqrt{s}$ for $P_{\text{eff}} = -1, -0.5, 0, +0.5, +1$ (notation as in Fig. 1).

FIG. 17. Total NLO top quark polarization averaged over the forward and backward hemispheres for $P_{\text{eff}} = -1, 0, +1$ as a function of $\sqrt{s}$.

$$P^{(\ell)} = -\left(1 - \frac{\alpha_s}{3\pi}\left(\frac{f_{RR}^2}{f_{RL}^2} + [2]\right) + \cdots\right), \quad (58)$$

where the bracketed notation "[2]" denotes the anomalous contribution not present in $m_t/\sqrt{s} = 0$ production (see Ref. [28]). Using $f_{RR}^2/f_{RL}^2 = 16.069$ and $\alpha_s(3000 \text{ GeV}) = 0.079$ the radiative correction at the backward point amounts to 15% which is reasonably close to the value in Fig. 15(b). The anomalous contribution is quite small. The corresponding formula for Fig. 15(a) ($P_{\text{eff}} = -1$) is obtained from Eq. (58) by the substitution $f_{RR,RL} \rightarrow f_{LL,LR}$. With $f_{LL}^2 = 1.417$ and $f_{LR}^2 = 0.188$, one obtains a radiative correction of 8% at the backward point, again in approximate agreement with Fig. 15(a). One may state that the large radiative corrections at the backward point for $P_{\text{eff}} = \pm 1$ at $\sqrt{s} = 3000$ GeV result from the fact that $f_{RR} \gg f_{RL}$ and $f_{LL} \gg f_{LR}$.

Next we investigate the parameter space for which the polarization of the top quark is minimal. For some measurements it may be advantageous to eliminate or minimize polarization effects. For once, one can thereby gauge the efficiency of a polarization measurement against an unpolarized control sample. The parameters to be varied are the effective beam polarization P_{eff}, the polar angle θ, and the energy $\sqrt{s}$. The minimization is done at NLO including the normal polarization component according to Eq. (57).

In Fig. 18(a) we show a plot of the NLO values of P_{eff} which minimize $|\vec{P}|$ for any given scattering angle. The minimizing values $P_{\text{eff}}^{\text{min}}$ depend in addition on the energy. An important feature of the minimizing effective beam polarization is that, in the forward region, where the rate is largest, the dependence of $P_{\text{eff}}^{\text{min}}$ on $\cos\theta$ is reasonably flat for all shown energies. This means that it is possible to tune the effective beam polarization in the forward region for each energy such that one obtains approximate minimal polarization. Just above threshold at $\sqrt{s} = 360$ GeV, $P_{\text{eff}}^{\text{min}}$ is close to the flat behavior at threshold $P_{\text{eff}}^{\text{min}} = A_{RL} = 0.409$. Apart from the near-threshold curve $P_{\text{eff}}^{\text{min}}$ shows a
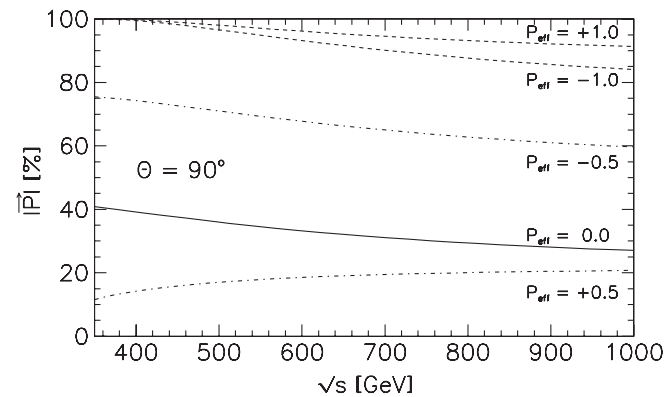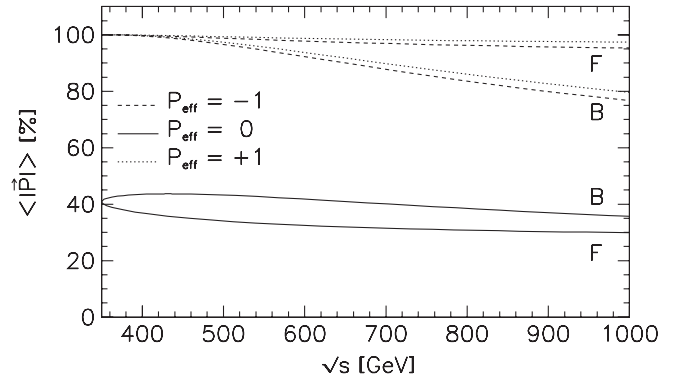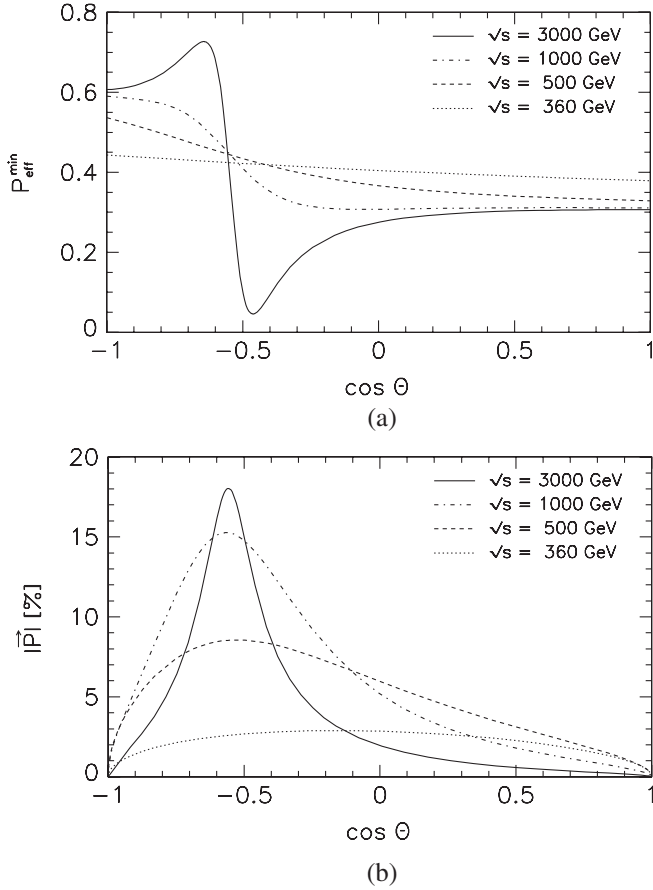
FIG. 18. (a) P_{eff} values required for minimal top quark polarization $|\vec{P}|$ and (b) minimal values for $|\vec{P}|$, plotted against $\cos\theta$, for $\sqrt{s} = 360$, 500, 1000, and 3000 GeV notation as in Fig. 5).
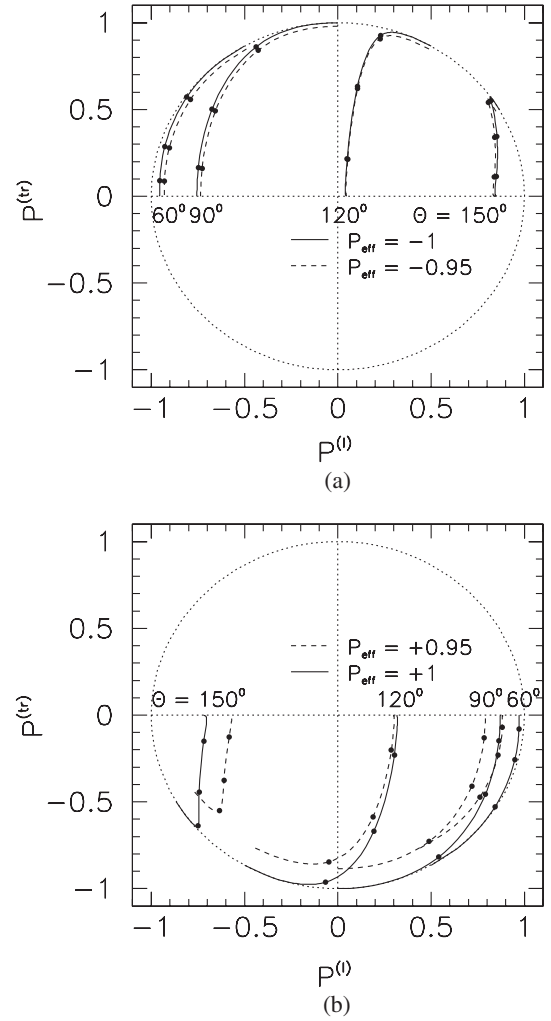

FIG. 19. NLO Parametric plot of the orientation and the length of the polarization vector in dependence on the c.m. energy $\sqrt{s}$ for values $\theta = 60°$, $90°$, $120°$, and $150°$ for (a) $P_{\text{eff}} = -1$ (solid lines) and $P_{\text{eff}} = -0.95$ (dashed lines), and (b) $P_{\text{eff}} = +1$ (solid lines) and $P_{\text{eff}} = +0.95$ (dashed lines). The dots on the trajectories from the border to the central line stand for $\sqrt{s} = 500$, 1000, and 3000 GeV.

strong dependence on $\cos\theta$ in the backward region. The corresponding minimal values of $|\vec{P}|$ are shown in Fig. 18 (b). At the forward and backward point the minimal polarization is zero by construction. In the forward region the polarization remains quite small starting from zero at the forward point. This is different in the backward region where the minimal polarization can become as large as 18% for the highest shown energy of $\sqrt{s} = 3000$ GeV.

We now turn to the orientation of the polarization vector. We have already discussed some aspects of the orientation of the polarization vector of the top quark in Secs. IV and V. We now combine the information on the orientation and the magnitude of the polarization vector in one single (radius, angle) plot where we trace the end point (apex) of the polarization vector $\vec{P}$ within the unit circle while increasing the energy from threshold to infinity. The apex stays within the unit circle since $|\vec{P}| \leq 1$. In Fig. 19(a) we consider the case $P_{\text{eff}} = -1$ for the polar angles $\theta = 60°$, $90°$, $120°$, and $150°$. All trajectories start off at threshold where $|\vec{P}| = 1$ and $\alpha = 180° - \theta$ and, depending on $\cos\theta$, end up at $\alpha = 0°$ or $\alpha = 180°$ with a length close to the asymptotic Born term result [Eq. (34)]. Which of the two

asymptotic solutions $\alpha = 0°$ and $\alpha = 180°$ are attained can be traced to the corresponding LO result [Eq. (34)] or from Fig. 7(b). For $P_{\text{eff}} = +1$ [Fig. 19(b)] the trajectories start off at threshold with $\alpha = -\theta$ and end up at $\alpha = 0°$ or $\alpha = 180°$. The appropriate solution can again be read off from the Born term formula [Eq. (34)] with the appropriate replacements as described after Eq. (34), or from Fig. 7(b). The length of the asymptotic polarization vector is close to what is obtained from Eq. (34) after the appropriate replacements. Since $f_{LR}^2/f_{LL}^2 > f_{RL}^2/f_{RR}^2$ the asymptotic values of $|\vec{P}|$ and thereby the intermediate values of $|\vec{P}|$ are larger for $P_{\text{eff}} = +1$ than for $P_{\text{eff}} = -1$. We remind the reader, though, that extrapolations away from $P_{\text{eff}} = -1$ are more stable than extrapolations away from $P_{\text{eff}} = +1$. This is illustrated in Figs. 19(a) and 19(b) by adding the

corresponding trajectories (dashed lines) for $P_{\text{eff}} = -0.95$ and $P_{\text{eff}} = +0.95$, respectively. One observes only a minor change in Fig. 19(a) going from $P_{\text{eff}} = -1$ to $P_{\text{eff}} = -0.95$. For example, the total polarization $|\vec{P}|$ remains close to maximal at $\sqrt{s} = 500$ GeV for the technically feasible effective beam polarization of $P_{\text{eff}} = -0.95$. The corresponding changes in Fig. 19(b) are much larger. In particular, the total polarization $|\vec{P}|$ at $P_{\text{eff}} = +0.95$ is considerably reduced from its values at $P_{\text{eff}} = +1$.

In Figs. 19(a) and 19(b) we have marked the energy dependence of the polarization vector by dots (or ticks) on the trajectory of the apex of the polarization vector. One notes that there is very little change in the length of the polarization vector going from threshold to $\sqrt{s} = 500$ GeV. The ticks are approximately equally spaced on the trajectories indicating an approximate inverse power law dependence of the spacing on the energy. For the three trajectories $\theta = 60°$, $90°$ and $120°$, the angle α is monotonically increasing with energy. In contrast to this the $\theta = 150°$ trajectory shows a kink at around $\sqrt{s} = 500$ GeV. Both Figs. 19(a) and 19(b) show that at $\sqrt{s} = 3000$ GeV one has not yet reached the asymptotic regime.

VIII. LONGITUDINAL SPIN-SPIN CORRELATIONS

Up to this point we have only discussed the single-spin polarization of the top quark. The polarizations of pair produced top and antitop quarks are correlated and could be observed in the energy spectra of decay products, especially in the energy spectra of leptons and antileptons. There are altogether nine double-density matrix elements describing the spin-spin correlations of the top and antitop quarks. Here we concentrate on the longitudinal spin-spin correlation which is the double-density matrix element that survives in the high-energy limit (for analytical NLO results see Refs. [28–30]). We mention that the full set of NLO double-density matrix elements has been numerically evaluated in Refs. [31,32].

The longitudinal spin-spin correlation cross section is defined by

$$\sigma_\alpha^{(\ell_1\ell_2)} = \sigma_\alpha(\uparrow\uparrow) - \sigma_\alpha(\uparrow\downarrow) - \sigma_\alpha(\downarrow\uparrow) + \sigma_\alpha(\downarrow\downarrow), \quad (59)$$

where e.g. $(\uparrow\uparrow)$ denotes a top quark with helicity $1/2$ and an antitop quark with helicity $1/2$, etc. Similar to Eq. (5), the differential $\cos\theta$ distribution is given by

$$\frac{d\sigma^{(\ell_1\ell_2)}}{d\cos\theta} = \frac{3}{8}(1 + \cos^2\theta)\sigma_U^{(\ell_1\ell_2)} + \frac{3}{4}\sin^2\theta\sigma_L^{(\ell_1\ell_2)}$$
$$+ \frac{3}{4}\cos\theta\sigma_F^{(\ell_1\ell_2)}, \quad (60)$$

where

$$\sigma_{U,L}^{(\ell_1\ell_2)} = (1 - h_-h_+)\frac{\pi\alpha^2 v}{3q^4}((g_{11} + P_{\text{eff}}g_{41})H_{U,L}^{1(\ell_1\ell_2)}$$
$$+ (g_{12} + P_{\text{eff}}g_{42})H_{U,L}^{2(\ell_1\ell_2)}),$$

$$\sigma_F^{(\ell_1\ell_2)} = (1 - h_-h_+)\frac{\pi\alpha^2 v}{3q^4}(g_{44} + P_{\text{eff}}g_{14})H_F^{4(\ell_1\ell_2)}. \quad (61)$$

The Born term contributions read [28]

$$H_U^{1(\ell_1\ell_2)}(\text{Born}) = -2N_c q^2(1 + v^2),$$
$$H_L^{1(\ell_1\ell_2)}(\text{Born}) = N_c q^2(1 - v^2) = H_L^{2(\ell_1\ell_2)}(\text{Born}),$$
$$H_U^{2(\ell_1\ell_2)}(\text{Born}) = -2N_c q^2(1 - v^2), \quad (62)$$
$$H_F^{4(\ell_1\ell_2)}(\text{Born}) = -4N_c q^2 v.$$

Note that one has the Born term relations

$$H_U^{1,2}(\text{Born}) = -H_U^{1,2(\ell_1\ell_2)}(\text{Born}),$$
$$H_F^4(\text{Born}) = -H_F^{4(\ell_1\ell_2)}(\text{Born}), \quad (63)$$
$$H_L^{1,2}(\text{Born}) = H_L^{1,2(\ell_1\ell_2)}(\text{Born}),$$

which are due to angular momentum conservation in the back-to-back configuration of the Born term production [28]. These relations no longer hold true in the case of additional gluon emission. The relations (63) imply that $P^{(\ell_1\ell_2)} = -1$ at $\cos\theta = \pm 1$ independent of P_{eff}. Since the transverse contributions $H_{U,F}$ dominate over the longitudinal contributions H_L, one anticipates from the relations (63) that the longitudinal spin-spin correlations are negative and only weakly beam polarization dependent.

Similar to Eq. (18), the $\cos\theta$ dependent longitudinal spin-spin correlation is defined by the ratio

$$P^{(\ell_1\ell_2)}(\cos\theta) = \frac{N^{(\ell_1\ell_2)}(\cos\theta)}{D(\cos\theta)}, \quad (64)$$

with the denominator function given in Eq. (22). The numerator function is given by

$$N^{(\ell_1\ell_2)}(\cos\theta) = \frac{3}{8}(1 + \cos^2\theta)((g_{11} + g_{41}P_{\text{eff}})H_U^{1(\ell_1\ell_2)}$$
$$+ (g_{12} + g_{42}P_{\text{eff}})H_U^{2(\ell_1\ell_2)})$$
$$+ \frac{3}{4}\sin^2\theta((g_{11} + g_{41}P_{\text{eff}})H_L^{1(\ell_1\ell_2)}$$
$$+ (g_{12} + g_{42}P_{\text{eff}})H_L^{2(\ell_1\ell_2)})$$
$$+ \frac{3}{4}\cos\theta(g_{44} + g_{14}P_{\text{eff}})H_F^{4(\ell_1\ell_2)}. \quad (65)$$

Let us first consider the polar angle average of the longitudinal spin-spin correlation. For the Born term contribution, one obtains

$$\langle P^{(\ell_1\ell_2)}\rangle = -\frac{1}{3}\frac{(g_{11}+P_{\mathrm{eff}}g_{41})(1+3v^2)+(g_{12}+P_{\mathrm{eff}}g_{42})(1-v^2)}{(g_{11}+P_{\mathrm{eff}}g_{41})(1+v^2/3)+(g_{12}+P_{\mathrm{eff}}g_{42})(1-v^2)}. \tag{66}$$

Note that $\langle P^{(\ell_1\ell_2)}\rangle = -1/3$ at threshold ($v = 0$) and $\langle P^{(\ell_1\ell_2)}\rangle = -1$ in the high-energy limit ($v = 1$) independent of the beam polarization parameter P_{eff}. In fact, the dependence on P_{eff} is very weak also for energies intermediate between these two limits. For example, for $\sqrt{s} = 500$ GeV one finds

$$\langle P^{(\ell_1\ell_2)}\rangle = \langle P^{(\ell_1\ell_2)}\rangle(P_{\mathrm{eff}} = 0)\frac{1-0.36P_{\mathrm{eff}}}{1-0.37P_{\mathrm{eff}}}$$

$$= \begin{cases} -0.67 & P_{\mathrm{eff}} = +1 \\ -0.65 & = 0 \\ -0.65 & = -1 \end{cases}. \tag{67}$$

Equation (67) shows that the dependence on the beam polarization parameter P_{eff} practically drops out in the ratio (67).

In Fig. 20 we plot the average longitudinal spin-spin correlation function $\langle P^{(\ell_1\ell_2)}\rangle$ up to $O(\alpha_s)$ as a function of $\sqrt{s}$ for different effective beam polarizations. The dependence of $\langle P^{(\ell_1\ell_2)}\rangle$ on P_{eff} is barely visible.

As shown in Ref. [5] the off-diagonal basis defined by Eq. (39) diagonalizes both the single-spin and the spin-spin double-density matrix at the Born term level for $P_{\mathrm{eff}} = -1$. In the NLO calculation described in this section, the top and antitop quark are no longer back to back due to hard gluon emission, i.e. in the two helicity basis (top and antitop quark) the two respective z axis are not in general back to back. In the high-energy limit, where only the longitudinal spin-spin density matrix elements survive, the NLO spin-spin density matrix elements are therefore not simply related to the off-diagonal basis introduced in Ref. [5]. A discussion of the rigidity of back-to-back ($t\bar{t}$) pairs with respect to gluon emission in e^+e^- collisions can be found in Ref. [33].
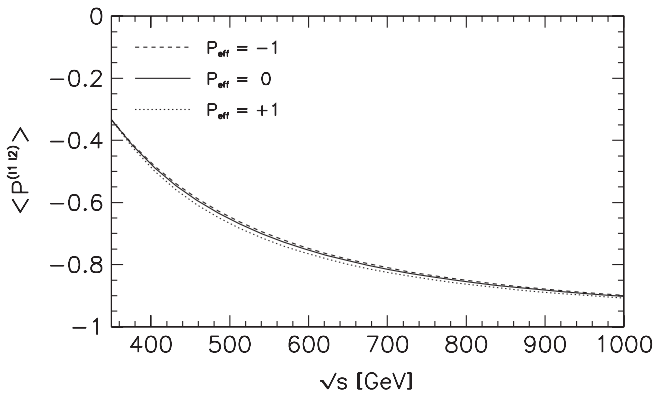

FIG. 20. NLO beam energy dependence of the polar average of the longitudinal spin-spin correlation function $\langle P^{(\ell_1\ell_2)}\rangle$.

IX. SUMMARY AND CONCLUSIONS

We have discussed in detail top quark polarization in above-threshold ($t\bar{t}$) production at a polarized linear e^+e^- collider within the SM. While journeying through the three-dimensional $(P_{\mathrm{eff}}, \cos\theta, \sqrt{s})$-parameter space a rich landscape of SM polarization phenomena unfolds which awaits experimental confirmation or falsification. Generally speaking, one needs large values of the effective beam polarization if the aim is to produce highly polarized top quarks. Very small or zero polarization of the top quark can be obtained by fine-tuning the parameters $(P_{\mathrm{eff}}, v, \cos\theta)$.

The ($t\bar{t}$)-production rate at a polarized linear e^+e^- collider is governed by the gain factor $K_G = 1 - h_-h_+$ and the effective beam polarization P_{eff}. The optimal choice as concerns the rate is h_- negative and h_+ positive such that one has $K_G > 1$ and $P_{\mathrm{eff}} < 0$, i.e. the optimal choice for the rate would lie in the second quadrant of the (h_-, h_+) plane in Fig. 3. The largest gain in the rate is obtained for $h_- = -h_+ = -1$, i.e. for $K_G = 2$ and $P_{\mathrm{eff}} = -1$.

At (Born term) threshold, one has a flat $\cos\theta$ distribution. As the energy increases there is a quick turn into forward dominance, with little dependence on P_{eff}. This is a welcome feature for polarization measurements, which require large statistics and rates, since forward production is advantageous for stable and large top quark spin effects. More explicitly, the polarization of the top quark is generally large and more stable against variations of the parameters P_{eff}, $\cos\theta$ and the energy in the forward region than in the backward region.

Contrary to the rate, the polarization observables depend only on P_{eff}, and not separately on h_- and h_+. We find that the single-spin polarization of the top quark is, in general, strongly dependent on the effective beam polarization parameter P_{eff}. This is quite different for longitudinal spin-spin correlations which depend only weakly on beam polarization effects.

In order to attain small or large values of the polarization would in general require an extreme fine-tuning of P_{eff} depending on $\cos\theta$ and the energy. The good news is that the polarization properties at $\sqrt{s} = 500$ GeV are still quite close to the polarization properties at threshold where they are quite simple. If the aim is to achieve zero or small polarization at $\sqrt{s} = 500$ GeV a choice of $P_{\mathrm{eff}} = 0.36 \div 0.40$ leads to very small values of $|\vec{P}|$ in the forward hemisphere where the rate is largest. At $\sqrt{s} = 500$ GeV, close to maximal values of the polarization $|\vec{P}| \simeq 1$ can be achieved over the whole $\cos\theta$ range for effective beam polarizations close to $P_{\mathrm{eff}} = -1$ or $P_{\mathrm{eff}} = +1$, where the polarization is slightly larger for $P_{\mathrm{eff}} = +1$. However, a

choice close to $P_{\text{eff}} = -1$ is preferred because of two reasons. First, this choice leads to larger rates and, second, the polarization observables are more stable against variations of P_{eff} close to $P_{\text{eff}} = -1$ than close to $P_{\text{eff}} = +1$. For $\sqrt{s} = 1000$ GeV a total polarization of $|\vec{P}| > 85\%$ and $|\vec{P}| > 90\%$ can be achieved in the forward hemisphere for $P_{\text{eff}} = -1$ and $P_{\text{eff}} = +1$, respectively. The highest energy considered in this paper is $\sqrt{s} = 3000$ GeV. We have found that the polarization results at $\sqrt{s} = 3000$ GeV are, in many aspects, not very close to their respective asymptotic values.

For the analysis of polarization effects, one also needs to know the orientation of the polarization vector. We have given explicit results on its orientation where we have found that, at $\sqrt{s} = 500$ GeV, the polarization vector is still approximately aligned or counteraligned with the electron momentum as is the case at threshold.

Our results can be viewed as a generalization of the $P_{\text{eff}} = -1$ results of Ref. [5] to general values of $-1 \leq P_{\text{eff}} \leq +1$. We have checked that all our Born term formulas agree with those of Ref. [5] when we set $P_{\text{eff}} = -1$ in our Born term expressions. In addition, we have derived simple Born term rate and polarization formulas for the case $P_{\text{eff}} = +1$ not treated explicitly in Ref. [5]. We also provide $O(\alpha_s)$ corrections to the Born term results which we have checked against the corresponding $O(\alpha_s)$ corrections in the helicity system given in Ref. [6]. In addition, we provide radiative corrections to the orientation angle α of the polarization vector which were not discussed in Ref. [6].

All the results in this paper refer to the polarization of the top quark. In order to obtain the SM coupling predictions for the polarization of the antitop quark, let us first set up an orthonormal spin basis for the antitop quark by replacing the momenta in Eq. (4) by their charge conjugate partners, i.e. $\vec{p}_t \rightarrow \vec{p}_{\bar{t}}$ and $\vec{p}_{e^-} \rightarrow \vec{p}_{e^+}$. The three orthonormal basis vectors $(\vec{e}^{\,(\text{tr})}, \vec{e}^{\,(n)}, \vec{e}^{\,(\ell)})$ are now given by

$$\vec{e}^{\,(\text{tr})} = \frac{(\vec{p}_{e^+} \times \vec{p}_{\bar{t}}) \times \vec{p}_{\bar{t}}}{|(\vec{p}_{e^+} \times \vec{p}_{\bar{t}}) \times \vec{p}_{\bar{t}}|},$$

$$\vec{e}^{\,(n)} = \frac{\vec{p}_{e^+} \times \vec{p}_{\bar{t}}}{|\vec{p}_{e^+} \times \vec{p}_{\bar{t}}|}, \qquad (68)$$

$$\vec{e}^{\,(\ell)} = \frac{\vec{p}_{\bar{t}}}{|\vec{p}_{\bar{t}}|}.$$

In the polar angle distribution (5) the polar angle now refers to $\theta_{\bar{t}e^-}$ and *not* to $\theta = \theta_{te^-}$, as in the top quark case discussed in the main part of this paper. Since the lepton pair is back to back in the lab frame, one has $\theta_{\bar{t}e^-} = 180° - \theta_{\bar{t}e^+}$, i.e. the two terms in Eq. (5) proportional to $\cos\theta$ change sign if written in terms of $\cos\theta_{\bar{t}e^+}$. In the SM the rate and the polarization components of the antitop quark are related to those of the top quark via

$$\sigma_{\bar{t}}(\cos\theta_{\bar{t}e^+}) = \sigma_t(\cos\theta_{te^-}),$$

$$P_{\bar{t}}^{(\ell,n)}(\cos\theta_{\bar{t}e^+}) = -P_t^{(\ell,n)}(\cos\theta_{te^-}), \qquad (69)$$

$$P_{\bar{t}}^{(\text{tr})}(\cos\theta_{\bar{t}e^+}) = P_t^{(\text{tr})}(\cos\theta_{te^-}).$$

As an example, and as expected, the antitop quark is predominantly produced in the backward hemisphere relative to the e^- direction.

In polarized top decay the compositions of helicity fractions of the final state W^- bosons change relative to the helicity fractions of unpolarized top quark decay depending on the magnitude and orientation of the polarization vector. This polarization effect has been investigated in a number of papers where a variety of spin observables have been defined which involve the dominant decay mode of the top quark $t(\uparrow) \rightarrow b + W^+(\rightarrow \ell^+ + \nu_l)$. The analysis can be done in the (e^+e^-) c.m. frame as in Ref. [34], in the top quark rest frame as e.g. in Refs. [35–37], or in the W rest frame as e.g. in Refs. [3,38,39]. References [3,35,37,38] concentrate on SM predictions and discuss radiative QCD [3,35,38] corrections to the respective spin observables, while Ref. [34] analyzes the effect of non-SM interactions in the production and decay of the top quark. The authors of Ref. [39] discuss some novel spin observables and proceed to analyze the effect of non-SM decay vertices on these observables. QCD corrections to non-SM interactions in the decay of an unpolarized top quark have been recently calculated in Ref. [40]. This calculation can be easily extended to polarized top quark decay.

The discussion of this paper has focused on SM physics with longitudinal beam polarization. Non-SM electroweak couplings on the production side, involving leptons and quarks, and transverse beam polarization effects can be easily included using the formalism of this paper. Transverse beam polarization effects will be discussed in a sequel to this paper.

ACKNOWLEDGMENTS

APPENDIX: SM VALUES OF THE ELECTROWEAK COUPLING COEFFICIENTS

The electroweak coupling matrix elements $g_{ij}(s)$ needed in this paper are given by

$$g_{11/12} = Q_f^2 - 2Q_f v_e v_f \operatorname{Re}\chi_Z$$
$$+ (v_e^2 + a_e^2)(v_f^2 \pm a_f^2)|\chi_Z|^2 (= 0.61/0.34),$$

$$g_{14} = 2Q_f v_e a_f \operatorname{Re}\chi_Z - 2(v_e^2 + a_e^2)v_f a_f |\chi_Z|^2 (= -0.14),$$

$$g_{41/42} = 2Q_f a_e v_f \operatorname{Re}\chi_Z$$
$$- 2v_e a_e (v_f^2 \pm a_f^2)|\chi_Z|^2 (= -0.21/-0.17),$$

$$g_{44} = -2Q_f a_e a_f \operatorname{Re}\chi_Z + 4v_e a_e v_f a_f |\chi_Z|^2 (= 0.50),$$

where

$$\chi_Z(s) = \frac{gM_Z^2 s}{(s - M_Z^2 + iM_Z\Gamma_Z)}, \qquad \text{(A1)}$$

with M_Z and Γ_Z the mass and width of the Z^0 and $g = (16\sin^2\theta_W \cos^2\theta_W M_Z^2)^{-1} = 4.229 \times 10^{-5}$ GeV^{-2}, where we have used $\sin^2\theta_W = 0.23116$. Q_f are the charges of the final state quarks to which the electroweak currents directly couple; v_e and a_e, v_f, and a_f are the electroweak vector and axial vector coupling constants. For example, in the Weinberg-Salam model, one has $v_e = -1 + 4\sin^2\theta_W$, $a_e = -1$ for leptons, $v_f = 1 - \frac{8}{3}\sin^2\theta_W$, $a_f = +1$ for up-type quarks $(Q_f = +\frac{2}{3})$, and $v_f = -1 + \frac{4}{3}\sin^2\theta_W$, $a_f = -1$ for down-type quarks $(Q_f = -\frac{1}{3})$. The electroweak coupling coefficients g_{ij} are not independent. They satisfy the constraints

$$((g_{11} \pm g_{41})^2 - (g_{14} \pm g_{44})^2)^{1/2} = g_{12} \pm g_{42}. \qquad \text{(A2)}$$

In Eq. (A1) we have also listed the numerical values of the electroweak coefficients for $(t\bar{t})$ production at $\sqrt{s} = 500$ GeV. As already mentioned in the main text, it is safe to work in the zero width approximation for the Z boson above $(t\bar{t})$ threshold, i.e. we set $\Gamma_Z = 0$. Note that the numerical values of the electroweak coefficients are only weakly energy dependent above the $(t\bar{t})$ threshold. The energy dependence comes from the energy-dependent factor $\chi_Z(s)$ which takes the values 0.377, 0.364, and 0.352 for $\sqrt{s} = 350$ GeV (threshold), 500 GeV, and infinite energy, respectively.

For some applications it is convenient to switch to chiral representations of the initial and final electromagnetic and weak currents as was done in Ref. [5]. Accordingly, one defines coefficients

$$f_{LL/LR} = -Q_f + (v_e + a_e)(v_f \pm a_f)\chi_Z(s). \qquad \text{(A3)}$$

The chiral electroweak coefficients $f_{LL/LR}$ can be seen to be related to the above g_{ij} via

$$f_{LL/LR} = -(g_{11} \mp g_{14} - g_{41} \pm g_{44})^{1/2} \quad (= -1.21/-0.43),$$
$$f_{LL}f_{LR} = g_{12} - g_{42} \quad (= 0.51). \qquad \text{(A4)}$$

For the case $P_{\text{eff}} = +1$, one also needs the corresponding relations for the coefficients

$$f_{RR/RL} = -Q_f + (v_e - a_e)(v_f \mp a_f)\chi_Z(s). \qquad \text{(A5)}$$

One has

$$f_{RR/RL} = -(g_{11} \pm g_{14} + g_{41} \pm g_{44})^{1/2} \quad (= -0.87/-0.20),$$
$$f_{RR}f_{RL} = g_{12} + g_{42} \quad (= 0.18). \qquad \text{(A6)}$$

[1] J. E. Brau *et al.* (ILC Collaboration), arXiv:0712.1950.
[2] N. Phinney, N. Toge, and N. Walker, arXiv:0712.2361.
[3] M. Fischer, S. Groote, J. G. Körner, M. C. Mauser, and B. Lampe, Phys. Lett. B **451**, 406 (1999).
[4] V. Ravindran and W. L. van Neerven, Nucl. Phys. **B589**, 507 (2000).
[5] S. Parke and Y. Shadmi, Phys. Lett. B **387**, 199 (1996).
[6] J. Kodaira, T. Nasuno, and S. J. Parke, Phys. Rev. D **59**, 014023 (1998).
[7] R. W. Assmann *et al.*, Reports No. CERN-2000-008 and No. SLAC-REPRINT-2000-096.
[8] V. S. Fadin and V. A. Khoze, Yad. Fiz. **48**, 487 (1988) [JETP Lett. **46**, 525 (1987)].
[9] R. Harlander, M. Jeżabek, J. H. Kühn, and M. Peter, Z. Phys. C **73**, 477 (1997).
[10] M. Awramik and M. Jeżabek, Acta Phys. Pol. B **32**, 2115 (2001).
[11] G. Alexander *et al.*, Nucl. Instrum. Methods Phys. Res., Sect. A **610**, 451 (2009).
[12] G. A. Moortgat-Pick *et al.*, Phys. Rep. **460**, 131 (2008).
[13] J. G. Körner and D. H. Schiller, DESY Report No. 81-043, 1981.
[14] S. Groote, J. G. Körner, and M. M. Tung, Z. Phys. C **74**, 615 (1997).
[15] F. M. Renard, *Basics of Electron Positron Collisions* (Editions Frontieres, Dreux, France, 1981), p. 238; F. M. Renard, Z. Phys. C **45**, 75 (1989).
[16] K. I. Hikasa, Phys. Rev. D **33**, 3203 (1986).
[17] H. E. Haber, arXiv:hep-ph/9405376.
[18] J. H. Kühn, A. Reiter, and P. M. Zerwas, Nucl. Phys. **B272**, 560 (1986).
[19] J. G. Körner, A. Pilaftsis, and M. M. Tung, Z. Phys. C **63**, 575 (1994).
[20] S. Groote, J. G. Körner, and M. M. Tung, Z. Phys. C **70**, 281 (1996).
[21] S. Groote and J. G. Körner, Z. Phys. C **72**, 255 (1996); Eur. Phys. J. C **70**, 531 (2010).
[22] S. Groote and J. G. Körner, Phys. Rev. D **80**, 034001 (2009).
[23] J. H. Kühn, T. Hahn, and R. Harlander, arXiv:hep-ph/9912262.

[24] Y. S. Tsai, Phys. Rev. D **4**, 2821 (1971); **13**, 771 (1976).

[25] J. H. Kühn, DESY LC Notes, Report No. LC-TH-2001-004.

[26] S. Groote, H. Liivat, I. Ots, and T. Sepp, Eur. Phys. J. C **66**, 271 (2010).

[27] S. Groote, H. Liivat, and I. Ots, Nucl. Phys. **B843**, 213 (2011).

[28] S. Groote, J. G. Körner, and J. A. Leyva, Eur. Phys. J. C **63**, 391 (2009).

[29] M. M. Tung, J. Bernabeu, and J. Peñarrocha, Phys. Lett. B **418**, 181 (1998).

[30] S. Groote, J. G. Körner, and J. A. Leyva, Phys. Lett. B **418**, 192 (1998).

[31] A. Brandenburg, M. Flesch, and P. Uwer, Phys. Rev. D **59**, 014001 (1998).

[32] A. Brandenburg, M. Flesch, and P. Uwer, Czech. J. Phys. **50S1**, 51 (2000).

[33] S. Groote, J. G. Körner, and J. A. Leyva, Nucl. Phys. **B527**, 3 (1998).

[34] B. Grzadkowski and Z. Hioki, Nucl. Phys. **B585**, 3 (2000).

[35] A. Czarnecki, M. Jeżabek, J. G. Körner, and J. H. Kühn, Phys. Rev. Lett. **73**, 384 (1994).

[36] S. Groote, W. S. Huo, A. Kadeer, and J. G. Körner, Phys. Rev. D **76**, 014012 (2007).

[37] J. G. Körner and D. Pirjol, Phys. Rev. D **60**, 014021 (1999).

[38] M. Fischer, S. Groote, J. G. Körner, and M. C. Mauser, Phys. Rev. D **65**, 054036 (2002).

[39] J. A. Aguilar-Saavedra and J. Bernabeu, Nucl. Phys. **B840**, 349 (2010).

[40] J. Drobnak, S. Fajfer, and J. F. Kamenik, Phys. Rev. D **82**, 114008 (2010).